



Christoph Rieger, Bsc.

# **Hierarchical architectures for spiking Winner-Take-All networks**

## **Master's Thesis**

to achieve the university degree of

Master of Science

Master's degree programme: Biomedical Engineering

submitted to

**Graz University of Technology**

Supervisor

Univ.-Prof. Dipl.-Ing. Dr.techn. Robert Legenstein

Institute of Theoretical Computer Science

Head: Univ.-Prof. Dipl.-Ing. Dr.techn. Robert Legenstein

Graz, August 2023



---

## Abstract

This thesis explores hierarchical architectures of spiking Winner-Take-All (WTA) networks, with the focus on simulating feedback mechanisms found in the visual cortex. Such feedback mechanisms are related to attention and consistent beliefs across different areas of the visual cortex. First, the biological and theoretical concepts of spiking neural networks and their relationship to Bayesian inference are established. It is demonstrated how the hypothesized probabilistic nature of the brain can be linked to the model of a spiking WTA network that performs Bayesian inference. The thesis involves a series of experiments designed to test the network's response to visual stimuli. The response of the network to ambiguous images is tested and it is shown that the added feedback makes a crucial contribution to interpreting such images. An effect of the visual cortex of seeing illusory lines is reproduced by feeding the network feedback that contradicts the visual input. Furthermore, the model's link to Bayesian inference is verified by calculating conditional probabilities of neurons and then deriving their synaptic weights from them. To gain a better understanding of the network model the impact of the different network hyperparameters is analysed. An unexpected property of the firing frequencies of input and prior neurons is discovered, which changes the output's probability distribution of the network. The reusability of hyperparameters to networks of different sizes is tested. It is found that the hyperparameters are not universal to all network sizes. The quality of the training of the network was compared to the analytical optimum and it was found that the training could not reach it. These experiments combined reveal that incorporating feedback enhances the network's ability to process visual information, reflecting behaviours observed in biological systems.

---

## Kurzfassung

Diese Arbeit untersucht hierarchische Architekturen von gepulsten Winner-Take-All (WTA) Netzwerken, mit dem Fokus auf der Simulation von Rückkopplungsmechanismen, welche im visuellen Kortex gefunden wurden. Solche Rückkopplungsmechanismen hängen mit Aufmerksamkeit und einheitlichen Überzeugungen, über verschiedene Areale des visuellen Kortex hinweg, zusammen. Zunächst werden die biologischen und theoretischen Konzepte von gepulsten neuronalen Netzwerken und ihre Beziehung zur Bayesschen Inferenz gezeigt. Es wird verdeutlicht, wie die hypothetisierte probabilistische Natur des Gehirns mit dem Modell eines gepulsten WTA Netzwerks, welches Bayessche Inferenz durchführt, verknüpft werden kann. Die Arbeit umfasst eine Reihe von Experimenten, die entworfen wurden, um die Reaktion des Netzwerks auf visuelle Reize zu testen. Die Reaktion des Netzwerks auf mehrdeutige Bilder wird getestet und es wird gezeigt, dass das hinzugefügte Feedback einen entscheidenden Beitrag zur Interpretation solcher Bilder leistet. Der Effekt des visuellen Kortex, illusorische Linien zu sehen, wird reproduziert, indem dem Netzwerk Feedback gegeben wird, das den visuellen Reizen widerspricht. Außerdem wird der Zusammenhang zur Bayesschen Inferenz überprüft, indem die bedingten Wahrscheinlichkeiten von Neuronen berechnet werden und ihre synaptischen Gewichte von ihnen abgeleitet werden. Um ein besseres Verständnis des Netzwerkmodells zu gewinnen, wird der Einfluss von Hyperparametern des Netzwerks analysiert. Eine unerwartete Eigenschaft der Feuerraten der Eingangs- und Priorneuronen wird entdeckt, welche die Wahrscheinlichkeitsverteilung des Ausgangs des Netzwerks verändert. Die Wiederverwendbarkeit von Hyperparametern von Netzwerken unterschiedlicher Größen wird getestet. Es wird gezeigt, dass die Hyperparameter nicht universell auf alle Netzwerkgrößen anwendbar sind. Die Qualität des Trainings des Netzwerks wurde mit dem analytischen Optimum verglichen und es wurde gezeigt, dass das Training es nicht erreichen konnte. Diese Experimente in Verbindung zeigen, dass die Einbindung von Feedback die Fähigkeit des Netzwerks visuelle Informationen zu verarbeiten verbesserte und Verhaltensmuster widerspiegelt, die in biologischen Systemen beobachtet wurden.

# Contents

<b>Abstract</b>	<b>iii</b>
<b>Kurzfassung</b>	<b>iv</b>
<b>1 Introduction</b>	<b>1</b>
<b>2 Biological background</b>	<b>5</b>
2.1 Winner-Take-All networks . . . . .	5
2.2 The hierarchical structure of the brain . . . . .	6
2.3 Visual cortex . . . . .	6
2.4 Probabilistic brain . . . . .	8
2.5 Feedback in the visual cortex . . . . .	8
2.6 Synaptic plasticity . . . . .	10
2.7 Spiking neural networks . . . . .	11
<b>3 Theoretical background</b>	<b>13</b>
3.1 Bayes' theorem . . . . .	13
3.2 Bayesian inference . . . . .	13
3.3 Network model . . . . .	15
3.4 Mathematical link between the spiking Winner-Take-All network model and Bayesian inference . . . . .	21
<b>4 Experiments</b>	<b>25</b>
4.1 Experiment 1: Horizontal and vertical bars . . . . .	25
4.1.1 Introduction . . . . .	25
4.1.2 Methods . . . . .	25
4.1.3 Results . . . . .	28

## Contents

---

4.2	Experiment 2: Mathematical analysis and simulation of the network with 1-D images . . . . .	36
4.2.1	Introduction . . . . .	36
4.2.2	Methods . . . . .	37
4.2.3	Results . . . . .	41
4.3	Experiment 3: Transferability of hyperparameters . . . . .	57
4.3.1	Introduction . . . . .	57
4.3.2	Methods . . . . .	57
4.3.3	Results . . . . .	57
4.4	Experiment 4: Training of the network with 1-D images and predetermined hyperparameters . . . . .	60
4.4.1	Introduction . . . . .	60
4.4.2	Methods . . . . .	60
4.4.3	Results . . . . .	60
<b>5</b>	<b>Discussion</b>	<b>65</b>
5.1	Impact of the hyperparameters . . . . .	65
5.2	Basis of the network model . . . . .	67
5.3	Reproducing behaviours of the visual cortex . . . . .	68
5.4	Reusing hyperparameters for networks of different size . . . . .	69
5.5	Training weights with predetermined hyperparameters . . . . .	70
5.6	Future work . . . . .	70
	<b>Bibliography</b>	<b>73</b>

# List of Figures

2.1	Kanizsa square shown to the monkey by Lee TS (2003) . . . . .	9
3.1	Generative probabilistic model of the 3 node chain, representing the interaction of the inferior temporal cortex, V <sub>1</sub> and the visual input. It represents a multinomial mixture of 3 variables. X is a binary random vector of the visual input. Y is a multinomial variable of the output of V <sub>1</sub> and Z is a multinomial variable of the feedback of the inferior temporal cortex. X is assumed independent of Z, when Y is given, as the visual input is not influenced by the activity of the brain.	15
3.2	Architecture of the network. . . . .	16
3.3	Visualization of the kernel function $\varepsilon(s)$ within the relevant time window. A double exponential kernel was used. To limit the kernel function to positive values of s a Heaviside step function was applied. The output of this function was used to calculate the unweighed membrane potential response. . . . .	17
4.1	Generated training images. One image of each possible orientation at a random position. . . . .	26
4.2	Generated cross image, which can represent either horizontal or vertical orientation. . . . .	27

## List of Figures

---

- 4.3 **Training with 20 prior neurons.** **A** Examples of  $35 \times 35$ -pixel input images of horizontal and vertical bars with background noise. They were positioned without overlapping each others bars, thus showing the optimal areas output neurons should learn to respond to. **B** Learned weights of the connections between the input neurons, that were active for black pixels of the input image, and output neurons. As there was one such input neuron per pixel of the image the weights could be plotted in the same format as the image to easily interpret them. **C, D** Spike activity expressed by the output neurons before and after the training of the network. **E** Number of active output neurons during the presentation duration of each training image. **F** This shows the number of spikes the most active output neuron generated, relative to the number of spikes all other output neurons generated combined. . . . . 30
- 4.4 Learned weights of the connections between prior and output neurons. . . . . 31
- 4.5 **Horizontal validation.** Horizontal bars with a height of seven pixels were shown to the network at different positions. **A** Most active output neuron, depending on the vertical position of the center of a horizontal bar. **B** Output spikes during the validation process. The ticks of the x-axis are in steps of 0.2 seconds, thus each tick signifies the start of a new image being shown. **C** The mean number of active output neurons, depending on the vertical position of a horizontal bar. The standard deviation is given by the red bars. **D** This shows the number of spikes that the most active output neuron generated, relative to the number of spikes all other output neurons generated combined. The blue dots indicate the mean and the red bars the standard deviation. . . . . 33

4.6	<b>Vertical validation.</b> Vertical bars with a height of seven pixels were shown to the network at different positions. <b>A</b> Most active output neuron, depending on the horizontal position of the center of a vertical bar. <b>B</b> Output spikes during the validation process. The ticks of the x-axis are in steps of 0.2 seconds, thus each tick signifies the start of a new image being shown. <b>C</b> The mean number of active output neurons, depending on the horizontal position of a vertical bar. The standard deviation is given by the red bars. <b>D</b> This shows the number of spikes that the most active output neuron generated, relative to the number of spikes all other output neurons generated combined. The blue dots indicate the mean and the red bars the standard deviation. . . . .	34
4.7	<b>Impact of the prior Neurons.</b> <b>A</b> Validation image with a horizontal and a vertical bar on it. <b>B</b> Spiking activity of the output neurons with $z^v$ being active. <b>C</b> Spiking activity of the output neurons with $z^h$ being active. . . . .	35
4.8	<b>Cross image with varying prior neuron activity.</b> <b>A</b> Validation cross image. <b>B</b> Firing frequency of the 2 most active output neurons, depending on the firing frequency of $z^v$ . The output neuron firing frequencies were averaged over 10 runs to smooth the graphs. . . . .	37
4.9	<b>KL divergence for different <math>f_{input}</math> values.</b> Hyperparameters: $f_{prior} = 0\text{Hz}$ , $\tau_{decay} = 15\text{ms}$ . . . . .	42
4.10	<b>Analysis and simulation result.</b> Hyperparameters: $f_{input} = 42\text{Hz}$ , $f_{prior} = 0\text{Hz}$ , $\tau_{decay} = 15\text{ms}$ <b>A</b> Input images with $9 \times 1$ pixels, active pixels in black. <b>B</b> Analytically calculated posterior probabilities and simulated posterior probabilities. The standard deviations are given by the black bars. . . . .	43
4.11	<b>Analysis and simulation result.</b> Hyperparameters: $f_{input} = 70\text{Hz}$ , $f_{prior} = 0\text{Hz}$ , $\tau_{decay} = 15\text{ms}$ <b>A</b> Input images with $9 \times 1$ pixels, active pixels in black. <b>B</b> Analytically calculated posterior probabilities and simulated posterior probabilities. The standard deviations are given by the black bars. . . . .	45
4.12	<b>KL divergence for different <math>f_{input}</math> values.</b> Hyperparameters: $f_{prior} = 0\text{Hz}$ , $\tau_{decay} = 4\text{ms}$ . . . . .	46

## List of Figures

---

4.13	<b>Analysis and simulation result.</b> Hyperparameters: $f_{input} = 88\text{Hz}$ , $f_{prior} = 0\text{Hz}$ , $\tau_{decay} = 4\text{ms}$ <b>A</b> Input images with $9 \times 1$ pixels, active pixels in black. <b>B</b> Analytically calculated posterior probabilities and simulated posterior probabilities. The standard deviations are given by the black bars. . . . .	47
4.14	<b>KL divergence for different <math>f_{prior}</math> values.</b> Hyperparameters: $f_{input} = 42\text{Hz}$ , $\tau_{decay} = 15\text{ms}$ . . . . .	48
4.15	<b>Analysis and simulation result, active pixels in black.</b> Hyperparameters: $f_{input} = 42\text{Hz}$ , $f_{prior} = 222\text{Hz}$ , $\tau_{decay} = 15\text{ms}$ <b>A</b> Input images with $9 \times 1$ pixels. Prior given as red border. <b>B</b> Analytically calculated posterior probabilities and simulated posterior probabilities. The standard deviations are given by the black bars. . . . .	49
4.16	<b>KL divergence for different <math>f_{prior}</math> values.</b> Hyperparameters: $f_{input} = 88\text{Hz}$ , $\tau_{decay} = 4\text{ms}$ . . . . .	50
4.17	<b>Analysis and simulation result.</b> Hyperparameters: $f_{input} = 88\text{Hz}$ , $f_{prior} = 440\text{Hz}$ , $\tau_{decay} = 4\text{ms}$ <b>A</b> Input images with $9 \times 1$ pixels, active pixels in black. Prior given as red border. <b>B</b> Analytically calculated posterior probabilities and simulated posterior probabilities. The standard deviations are given by the black bars. . . . .	51
4.18	<b>Analysis and simulation result.</b> Hyperparameters: $f_{input} = 88\text{Hz}$ , $f_{prior} = 600\text{Hz}$ , $\tau_{decay} = 4\text{ms}$ <b>A</b> Input images with $9 \times 1$ pixels, active pixels in black. Prior given as red border. <b>B</b> Analytically calculated posterior probabilities and simulated posterior probabilities. The standard deviations are given by the black bars. . . . .	53
4.19	<b>KL divergence for different <math>f_{input}</math> values.</b> Hyperparameters: $f_{prior} = 440\text{Hz}$ , $\tau_{decay} = 4\text{ms}$ . . . . .	54
4.20	<b>Analysis and simulation result.</b> Hyperparameters: $f_{input} = 98\text{Hz}$ , $f_{prior} = 440\text{Hz}$ , $\tau_{decay} = 4\text{ms}$ <b>A</b> Input images with $9 \times 1$ pixels, active pixels in black. Prior given as red border. <b>B</b> Analytically calculated posterior probabilities and simulated posterior probabilities. The standard deviations are given by the black bars. . . . .	55

4.21	<b>Analysis and simulation result.</b> Hyperparameters: $f_{input} = 98\text{Hz}$ , $f_{prior} = 880\text{Hz}$ , $\tau_{decay} = 4\text{ms}$ <b>A</b> Input images with $18 \times 1$ pixels, active pixels in black. Prior given as red border. <b>B</b> Analytically calculated posterior probabilities and simulated posterior probabilities. The standard deviations are given by the black bars. . . . .	59
4.22	<b>KL divergence for different c values</b> $f_{input} = 98\text{Hz}$ , $f_{prior} = 440\text{Hz}$ , $\tau_{decay} = 4\text{ms}$ . . . . .	61
4.23	<b>Training result.</b> Hyperparameters: $f_{input} = 98\text{Hz}$ , $f_{prior} = 440\text{Hz}$ , $\tau_{decay} = 4\text{ms}$ , $c = 3$ <b>A</b> The learned probability matrix $P^{X Y}$ . It was determined by taking the weights to the power of e. <b>B</b> The calculated probability matrix $P^{X Y}$ . <b>C</b> The learned prior probability matrix $P^{Y Z}$ . <b>D</b> The calculated prior probability matrix $P^{Y Z}$ . <b>E, F</b> Spike activity expressed by the output neurons before and after the training of the network. <b>G</b> This shows the number of spikes the most active output neuron generated, relative to the number of spikes all other output neurons generated combined. . . . .	62
4.24	<b>Analysis and simulation result.</b> Hyperparameters: $f_{input} = 98\text{Hz}$ , $f_{prior} = 440\text{Hz}$ , $\tau_{decay} = 4\text{ms}$ , $c = 3$ <b>A</b> Input images with $9 \times 1$ pixels, active pixels in black. Prior given as red border. <b>B</b> Analytically calculated posterior probabilities and simulated posterior probabilities. The standard deviations are given by the black bars. . . . .	63



# List of Tables

4.1	<b>Analysis and simulation output probabilities.</b> Hyperparameters: $f_{input} = 42\text{Hz}, f_{prior} = 0\text{Hz}, \tau_{decay} = 15\text{ms}$ . . . . .	42
4.2	<b>Analysis and simulation output probabilities.</b> Hyperparameters: $f_{input} = 70\text{Hz}, f_{prior} = 0\text{Hz}, \tau_{decay} = 15\text{ms}$ . . . . .	44
4.3	<b>Analysis and simulation output probabilities.</b> Hyperparameters: $f_{input} = 88\text{Hz}, f_{prior} = 0\text{Hz}, \tau_{decay} = 4\text{ms}$ . . . . .	46
4.4	<b>Analysis and simulation output probabilities.</b> Hyperparameters: $f_{input} = 42\text{Hz}, f_{prior} = 222\text{Hz}, \tau_{decay} = 15\text{ms}$ . . . . .	50
4.5	<b>Analysis and simulation output probabilities.</b> Hyperparameters: $f_{input} = 88\text{Hz}, f_{prior} = 440\text{Hz}, \tau_{decay} = 4\text{ms}$ . . . . .	52
4.6	<b>Analysis and simulation output probabilities.</b> Hyperparameters: $f_{input} = 88\text{Hz}, f_{prior} = 600\text{Hz}, \tau_{decay} = 4\text{ms}$ . . . . .	54
4.7	<b>Analysis and simulation output probabilities.</b> Hyperparameters: $f_{input} = 98\text{Hz}, f_{prior} = 440\text{Hz}, \tau_{decay} = 4\text{ms}$ . . . . .	56
4.8	<b>Analysis and simulation output probabilities.</b> Hyperparameters: $f_{input} = 98\text{Hz}, f_{prior} = 880\text{Hz}, \tau_{decay} = 4\text{ms}$ . . . . .	58
4.9	<b>Analysis and simulation output probabilities.</b> Hyperparameters: $f_{input} = 98\text{Hz}, f_{prior} = 440\text{Hz}, \tau_{decay} = 4\text{ms}, c = 3$ . .	61



# 1 Introduction

Functional networks of the human brain have a hierarchical modular organization. This means the execution of one specific task, for example vision, involves several modules, which are interconnected (Meunier et al., 2009). Traditional views of the visual pathway of the brain hypothesized that the sensory input is passed on from lower to higher visual areas in a feed-forward system. However, Lee TS (2003) shows neurophysiological experimental evidence that there is feedback from high-level to low-level areas of the visual cortex. That feedback information is thought to be "explaining away" information, or putting emphasis on specific information of the low-level area. Through this mechanism, attention can be realized and different cortical areas are able to adopt the same interpretation of input.

The brain needs to handle a high degree of uncertainty in sensory input. When it first receives input it does not know what the information could represent, thus not knowing which parts of the input are most relevant. Several experiments on animals show that the computation of sensory input by the cerebral cortex can be explained and modelled by Bayesian inference (Funamizu Akihiro, 2016; Lee TS, 2003; Parr and Friston, 2018). They hypothesize that the brain functions in a generative and probabilistic way to reach its conclusions. This implies, that the brain expresses information via probability distributions, rather than utilizing static neural codes. Bayes theorem yields a posterior probability, by multiplying a likelihood with a prior probability. In cortical computation the posterior is represented by the output of a neural network. The likelihood can be computed based on the sensory input to the network. The feedback from high-level to low-level cortical areas can be modelled as the prior probability (Nessler et al., 2013).

There are various models for the computational dynamics of biological neurons (Gerstner and Kistler, 2002). One model, which is well supported, is

## 1 Introduction

---

the spiking neural network. This model aims to resemble biological neural networks more closely than common artificial neural networks. It generates neuron spikes, which increase the membrane potentials of other neurons they are connected to. The impact those neuron spikes have, is modelled by synaptic weights. Changes of these weights during learning are often modelled via Spike Timing Dependent Plasticity (STDP), which takes the exact timing of pre- and postsynaptic spikes into account. This form of plasticity agrees with biological experiments (Feldman, 2012; Dan Yang, 2004). To select the output of a neural network the soft Winner-Take-All mechanism is well established. Neurons with this mechanism choose what information is forwarded vertically into another layer and inhibit their horizontal neighbours of the same layer. This mechanism resembles the way biological pyramidal neurons function (Rodney J Douglas, 2004).

Nessler et al. (2013) and Guo et al. (2019) created spiking Winner-Take-All neural networks, which perform Bayesian inference. Both of those works did not include feedback that comes from a network higher up in the hierarchy. As such feedback is proven to exist by experiments, this thesis aims to expand the model. As a base, the hierarchical network model of Nessler et al. (2013) is used. This network is further expanded to simulate a spiking neural network that receives visual input and also feedback from another network higher up in the hierarchy.

In Chapter 2, the biological background of this thesis is given. The hierarchical structure of the brain is explained and further looked at via an example of hierarchy in the visual cortex. To better understand the example, a brief overview of the visual cortex is given first. An argument, supported by experiments, for the probabilistic brain is given. This argument is essential for this thesis, as the network model is of probabilistic nature. Finally synaptic plasticity and spiking neural networks are explained. The theoretical background, explaining the mathematical model used for the neural networks in this thesis, is explained in Chapter 3. In it, Bayesian inference is explained and how it can be applied to the example of hierarchical feedback in the visual cortex. After that, the network model is explained and all necessary equations are given. Finally, the link between the spiking Winner-Take-All network model and Bayesian inference is explained and shown. The various performed experiments are provided in Chapter 4. There are four different experiments that helped to analyse the network model and the aforemen-

---

tioned mathematical link between the model and Bayesian inference. The first experiment shows how the network can decide how to interpret ambiguous images with the help of the additional added feedback. This behaviour of the network can be interpreted as it setting attention on some part of an image. Further, it is shown how the output neurons learned to respond to specific areas of images through unsupervised learning. In the second experiment the conditional probabilities of the input and prior neurons are calculated and from those probabilities the weights of the network are determined. This proves the link between the spiking Winner-Take-All network model and Bayesian inference experimentally. Then the best network hyperparameters are searched and their influence on the network analysed. Furthermore, this experiment shows output for which there is no visual input, owed to the feedback. This behaviour is similar to the behaviour of seeing illusory lines observed in the visual cortex by Lee TS (2003). In Experiment 3 the transferability of network hyperparameters to networks of different sizes is tested. This proved impossible as the firing frequencies change the distribution of the output probabilities of the network. At last in Experiment 4 the best hyperparameters from Experiment 2 are used to train weights and to test how close to the analytical solution one can get by training the weights. Through that, problems in the training process of the network can be identified. Finally, in Chapter 5, the results and implications of the experiments are discussed.



## 2 Biological background

### 2.1 Winner-Take-All networks

It has been discovered that pyramidal neurons in the neocortex form selection networks (Rodney J Douglas, 2004). This means that one pyramidal neuron is allowed to fire, while others within the same layer are inhibited. This horizontal selection mechanism determines what is vertically sent on to the neurons of cortical layers higher up in the hierarchy. For example, there are pyramidal neurons that have a selection behaviour, which determines the subcortical output to motor structures (Rodney J Douglas, 2004). The inhibition of pyramidal neurons is performed by basket and chandelier cells (Rodney J Douglas, 2004). Basket cells connect to the soma of other neurons and control the action potential discharge rate of those neurons. Their dendritic branches wrap around the target soma, forming a "basket" giving them their name (Jones, 1984). Chandelier cells perform inhibition directly at the axonal initial segment of pyramidal neurons, where action potentials are initiated. (Contreras, 2004). The selection of one pyramidal neuron is called soft winner-take-all mechanism and is used in various neuronal network models (Rodney J Douglas, 2004). The mechanism is called "soft" because it uses a softmax function, which controls how many winners there can be, and how likely each neuron is to win (Arbib, 2003). It has been shown that winner-take-all mechanisms are computationally more powerful when compared to threshold gates (McCulloch-Pitts neurons) and sigmoidal gates. Furthermore, arbitrary continuous functions can be approximated by circuits that only include one soft winner-take-all gate as their only nonlinear operator (Maass, 2000).

## 2.2 The hierarchical structure of the brain

The brain is made up of modular structures that connect with each other in a hierarchical organization. These modules have a high level of connectivity within themselves and a low level to other modules. This means that there are different categories of neurons within a module, depending on their function in the network. For one there are provincial hub neurons that primarily connect to other neurons of the same module and are responsible for the function the module expresses. Then there are connector hub neurons that transfer information from the module to other modules. Such modules form networks, which are connected in a hierarchical manner, where each module is adding to the output of the previous module (Meunier et al., 2009). Most of the information flows upwards along the hierarchy, representing bottom-up observations. However, there is physiological experimental data that shows that information is also passed downwards. This influences the activity of modules lower in the hierarchy, representing top-down context (Lee TS, 2003). This will be explained for the visual cortex.

## 2.3 Visual cortex

The visual cortex is the region of the brain that processes visual information coming from the retina. From the retina the information is sent to the lateral geniculate nucleus in the thalamus and then further to visual area 1 (V1) of the visual cortex. The visual cortex consists of five visual areas (V1 to V5), which are divided by their function and structure. These areas are located in the occipital lobe of the cerebral cortex. The purpose of the visual areas is to process visual information to recognize objects, perform spatial tasks or to perform visual-motor skills. Neurons of the visual cortex often respond to stimuli within a specific receptive field. The receptive field of a neuron is comparable to the field of view of a human. Its size is given in degrees. It is assumed that each subsequent visual area is more specialized than the previous and due to that neurons in different visual areas can respond to the same receptive fields, but to different types of stimuli. There are various specialized cells in the visual cortex. For example, simple cells

and complex cells are well studied. Simple cells, which mainly occur in V1, respond primarily to oriented edges and lines within a receptive field. For example, a simple cell would always generate action potentials when there is a horizontal line in its receptive field. Complex cells can be found in V1, V2 and V3 and also respond primarily to oriented edges and lines. However, their receptive fields are larger and a horizontal edge, for example, does not have to be at a specific location in the receptive field to activate the cell. Some complex cells even respond primarily to movement of edges (Huff T, 2024). This activation of neurons, depending on the stimulus, is called neuronal tuning. The stimuli get more complex, the higher up in the visual cortex hierarchy they are located. For example, in the inferior temporal cortex, which receives visual information from V4, there are complex cells that respond to faces (Riesenhuber and Poggio, 2002). According to Palmer (1999) the larger receptive fields of complex cells are due to the hierarchical convergent nature of visual processing. This property follows from the complex cell receiving input from many simple cells, which is summed and integrated.

**The visual pathway** Visual information first enters the lateral geniculate nucleus (LGN). From there it is passed on to V1, which is the best-understood part of the visual cortex. It consists of six layers that function differently. Layer 4 receives the input from the LGN. It has the most simple cells of the six layers and thus processes visual information of small receptive fields. On layers 2, 3 and 6 there are complex cells, which combine the result of layer 4 into larger receptive fields. Through that, V1 outputs simple visual components with their orientation or direction. The processed information is then sent on to V2, which further processes it and thus responds to more visual complex patterns. V2 was also found to respond to differences in color and spatial frequency, additional to the more complex patterns and object orientation. After processing, V2 sends its information on to V3, V4 and V5. Furthermore, it also has feedback connections to V1. After V2 the visual information is split up into the dorsal and ventral streams, which each specialize in processing different features of the visual information. The dorsal stream is involved in guidance of motor actions and in recognizing where objects are in space. The ventral stream on the other hand is responsible for object recognition and form representation. (Huff T, 2024)

## 2.4 Probabilistic brain

When observing the activity of neurons during a task it varies from trial to trial. This suggests that no static neural code exists. It rather seems that the averaged activity of a neural network matters. Because of that, neuronal responses are typically treated statistically or probabilistically (Gerstner and Kistler, 2002). Pouget et al. (2013) state that there is strong behavioural and physiological evidence that the brain both represents probability distributions and performs probabilistic inference. Because of that, there are several experiments that support a mathematical framework based on Bayesian inference (see Chapter 3.2) to model brain computations. (Funamizu Akihiro, 2016; Lee TS, 2003; Parr and Friston, 2018; Darlington, Beck, and Lisberger, 2018). An advantage of these probabilistic models is their generality, meaning that they can be applied to various tasks that the brain performs (Pouget et al., 2013). Because of this evidence the neural network model of this thesis can be thought to perform Bayesian computation. The mathematical link between the spiking Winner-Take-All network model and Bayesian inference will be shown in Section 3.4.

## 2.5 Feedback in the visual cortex

Lee TS (2003) showed that feedback in the visual cortex is not only used for attentional selection or biased competition, but also to modulate the processing of the early visual cortex. Furthermore, they showed how this modulated processing can be explained via hierarchical Bayesian inference. One hypothetical example for the modulation of lower hierarchical areas that they give, is a human looking at a picture of a face, which is partially in shadow. First, V1 receives the information of the image and performs edge and line detection. In this initial processing the detected edges are in the well lit portion of the image, while in the shadowy part almost no edges are found. As this information is passed on upwards along the visual cortex hierarchy, it is processed further, until it reaches the inferior temporal cortex, where the conclusion is made that there is a face in the picture. After that, feedback is sent from the inferior temporal cortex back to V1. This

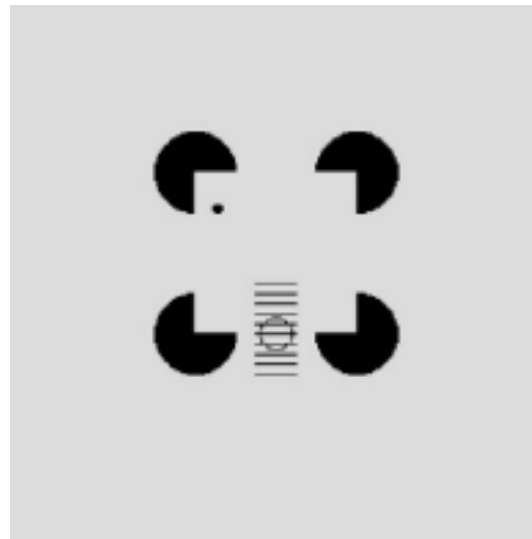


Figure 2.1: Kanizsa square shown to the monkey by Lee TS (2003)

feedback tells V1 that there should be edges hidden in the shadow. With this additional prior information V1 is able to detect the faint edge in the shadow and complete the contour of the face. In one of their experiments they made a monkey look at a fixation spot on a screen while Kanizsa squares were presented one at a time in different locations. Kanizsa squares are optical illusions, where an illusory square can be seen between four partial disks. One such image can be seen in Figure 2.1. The illusory square is seen, because the brain chooses the simplest interpretation that a white square is lying on top of the black circles, occluding them.

During the presentation, neuronal activity in V1 and V2 was measured. When looking at a single neuron in V1, which has a receptive field size of less than 0.8 degrees, they reported that it responds with increased spiking activity within 45 ms after a line appears in its receptive field. When that neuron has an illusory line of the Kanizsa square in its receptive field it is not active within 45 ms. However, after 100 ms it begins to respond, indicating that it starts seeing the illusory line. In contrast, the measured population of 39 V2 neurons responded to the illusory contour after 65 ms, 35 ms before V1. They explained this behaviour as V2 detecting the illusory contour with information from a spatially more global context and

then feeding back that information to V1. V1 then, convinced by V2, starts hallucinating the illusory line, agreeing with the most likely interpretation of the image. This experiment provides strong evidence that feedback is happening in the hierarchical structure of the visual cortex.

## 2.6 Synaptic plasticity

Electrophysiological experiments showed that the response amplitude of neurons changes over time (Markram et al., 1997). Depending on the stimulation a neuron receives, the postsynaptic response changes systematically. These changes can persist short term for hours or days. However, the stimulation paradigm can also induce persistent changes in the synapses of a neuron. These changes are supposed to reflect 'learning' and 'memory'. If the change increases the postsynaptic response it is called long-term potentiation (LTP). If it decreases the response it is called long-term depression (LTD). In neural network models a weight parameter between two neurons is used to indicate the strength of the postsynaptic response. When training a neural network model these weights can be adjusted to improve the performance of the network for a given task. By iteratively optimizing the weights the network learns to solve its task. Via a defined learning rule the network is able to determine the way in which to adapt the weights. There are different ways to define such a learning rule. One simple learning rule is to increase the weights of neurons that are more active than others. This is called Rate-Based Hebbian Learning. A more sophisticated learning rule is Spike Timing Dependent Plasticity (STDP). It also factors in the exact timing of presynaptic neuronal activity, compared to the timing of postsynaptic neuronal activity (Gerstner and Kistler, 2002). STDP is used to model the plasticity of this thesis' neural network model and will be explained further in the next section.

## 2.7 Spiking neural networks

Spiking neural networks (SNNs) are artificial neural networks that resemble biological neural networks more closely. Neurons in typical neural networks used in machine learning transmit information at every propagation cycle. This, however, is not how biological neurons operate. They generate action potentials (neuron spikes) to convey information between each other. These action potentials are only generated when their membrane potential exceeds a threshold. SNN models take this behaviour into account by keeping track of each neuron's membrane potential and then determining when they should produce an action potential (Gerstner and Kistler, 2002).

Previously, it was believed that biological neural networks encode information within the spike rates of neurons. However, neurobiological research shows evidence that at high speed processing this alone can not be sufficient. For example, image recognition tasks can be performed at a speed at which each neuron in the involved layers has only less than 10 ms to process the information. Such a time frame is too short for rate coding, as used in Hebbian Learning, to occur. Instead it has been shown that high speed processing tasks can be performed using the precise timing of spikes. Furthermore, it requires more energy for a neuron to spike many times to express a spike rate, rather than spiking just once and having the timing of the spike considered. This is a strong argument for spike timing encoded information, as the brain evolutionarily aims to minimize its energy consumption. The information encoding capacity is also higher in a small set of spiking neurons, compared to rate encoding. (Taherkhani et al., 2020) As a consequence of that, STDP is often used as learning rule in SNNs. STDP models the synaptic weight changes of neurons depending on the relative timing of pre- and postsynaptic spikes. If a presynaptic spike arrives shortly before the postsynaptic spike the synaptic weight is increased. The size of that increase depends exponentially on the time between both spikes, according to a time constant. However, when the presynaptic spike occurs after the postsynaptic spike the synaptic weight is decreased. These two mechanisms are called long-term potentiation and long-term depression, respectively. Although STDP is often modelled like this, biological experiments show that the standard pair-based approach does not fully explain it in biological neurons. (Taherkhani et al., 2020) Pfister and Gerstner (2006)

## [2 Biological background](#)

---

showed that pair-based STDP was not able to account for the dependence on the repetition frequency of pairs of spikes. However, there is experimental evidence that multiple-spike protocols, like triplets STDP, are more suitable to reproduce behaviour observed in neurons.

# 3 Theoretical background

## 3.1 Bayes' theorem

Bayes' theorem describes the probability of an event to occur, depending on the prior knowledge of conditions related to the event (Joyce, 2019)

$$P(A|B) = \frac{P(B|A)P(A)}{P(B)}, \quad (3.1)$$

where  $P(A|B)$  is the posterior probability of A, given that B is true.  $P(B|A)$  is called conditional probability of B, given A being true.  $P(A)$  is the prior probability, the probability of A occurring without any additional information. Finally  $P(B)$  is the marginal probability of B, without any given condition. This theorem is often used for Bayesian inference, where it expresses how a belief, which is represented as probability, changes due to related evidence.

## 3.2 Bayesian inference

Bayesian inference is a process of data analysis to calculate the probability of a hypothesis depending on the available related evidence. As over time more and more evidence becomes available the probabilities can be updated, yielding a more sophisticated view on the hypothesis. It is given, according to Bayes' theorem, by

$$P(H|E) = \frac{P(E|H)P(H)}{P(E)}, \quad (3.2)$$

### 3 Theoretical background

---

where  $H$  represents a hypothesis and  $E$  some related evidence.  $P(H|E)$  is the posterior probability, which signifies the probability of the hypothesis after the evidence was observed.  $P(E|H)$  is called likelihood and it is the probability of observing the evidence, given the hypothesis. It is a measure of the compatibility of the observed evidence with the given hypothesis.  $P(H)$  is the prior probability, which is the probability of the hypothesis before any evidence is considered or obtained.  $P(E)$  is called marginal likelihood that represents the probability of the evidence being observed. However, it is independent of the chosen hypothesis. Thus, it is not factored in when comparing different hypotheses. Bayesian inference can be applied to the "face in shadow" example of Section 2.5. There a neuron in  $V_1$  sees a small part of the visual field and signals if it sees an edge or not. At first it has the evidence of the observed pixels available and from it can calculate the likelihood that an edge is present. It has no prior knowledge of how probable an edge being present is, meaning that the prior probabilities for there being an edge or no edge are equal. With that likelihood and the prior probabilities it can conclude the posterior probability for the hypothesis "there is an edge" and decides that there is no edge. Later, the inferior temporal cortex determines that there is a face in the picture and feeds this information back to  $V_1$ . This influences the prior probabilities and changes the posterior probability. Through that, the  $V_1$  neuron starts to see the hypothesis "there is an edge" as more likely, in order to complete the contour of the face. We now define  $X$  as a binary random vector of the visual input,  $Y$  as a multinomial variable of the output of  $V_1$  and  $Z$  as a multinomial variable of the feedback of the inferior temporal cortex.  $X$  is assumed independent of  $Z$ , when  $Y$  is given, as the visual input is not influenced by the activity of the brain. This three node chain can be modelled as a generative probabilistic model and its visualization is given in Figure 3.1. In Section 3.2.2 of Korb and Nicholson (2011) it is shown how the chain rule can be applied to Bayesian Inference, when there are three nodes. When applying the chain rule and plugging the likelihood  $P(X|Y)$ , the prior  $P(Y|Z)$  and the prior distribution  $P(Z)$  into Equation 3.2, we get

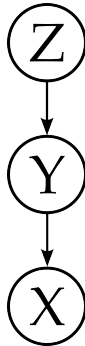


Figure 3.1: Generative probabilistic model of the 3 node chain, representing the interaction of the inferior temporal cortex, V1 and the visual input. It represents a multinomial mixture of 3 variables. X is a binary random vector of the visual input. Y is a multinomial variable of the output of V1 and Z is a multinomial variable of the feedback of the inferior temporal cortex. X is assumed independent of Z, when Y is given, as the visual input is not influenced by the activity of the brain.

the posterior  $P(Y|X, Z)$  as

$$\begin{aligned}
 P(Y = k|X = x, Z = j) &= \frac{P(X = x|Y = k)P(Y = k|Z = j)P(Z = j)}{\sum_{k'}P(X = x|Y = k')P(Y = k'|Z = j)P(Z = j)} \\
 &= \frac{P(X = x|Y = k)P(Y = k|Z = j)}{\sum_{k'}P(X = x|Y = k')P(Y = k'|Z = j)}. \tag{3.3}
 \end{aligned}$$

### 3.3 Network model

The network model used for the experiments in this thesis was taken from Nessler et al. (2013) and expanded by an additional layer to include hierarchical feedback information.

**Network architecture** Rectangular images in black and white were given to the network. These images had varying sizes in the experiments, determined by their width  $image_{width}$  and height  $image_{height}$ . Each pixel of an image was

### 3 Theoretical background

---

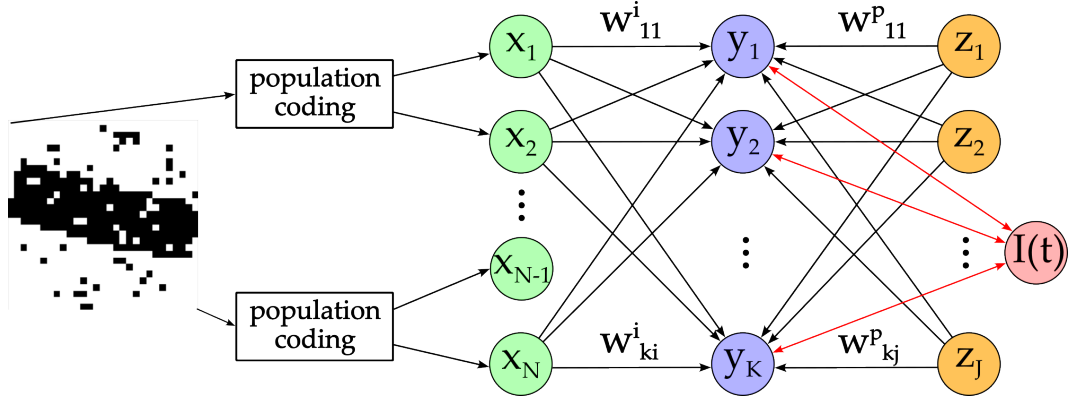


Figure 3.2: Architecture of the network.

connected to two neurons. The first of these neurons is in an active state when the pixel is black and in an inactive state otherwise. The second neuron expresses the opposite behaviour. As a consequence the network needs  $image_{width} \cdot image_{height} \cdot 2$  excitatory input neurons  $x_1, \dots, x_N$ . These input neurons are fully connected to the excitatory output neurons  $y_1, \dots, y_K$ . This means that every input neuron  $x_i$  is connected to each output neuron  $y_k$ . To simulate the feedback from the inferior temporal cortex prior neurons,  $z_1, \dots, z_J$ , were added to the network. The prior neurons were also fully connected to the output neurons. The output neurons are modelled in a soft winner-takes-all (soft-WTA) circuit. The WTA behaviour was implemented via an adaptive inhibition signal. The adaptive inhibition is used to regulate the membrane potentials of the output neurons so that all of them together fire with a total firing rate  $R(t) = 200\text{Hz}$  on average. Due to that, there never is a time window in which no output neuron may fire. However, it is unlikely for an output neuron to fire right after another output neuron has fired. A visualization of the network architecture can be seen in Figure 3.2.

**Neuron model** As in Nessler et al. (2013) the input neurons  $x_1, \dots, x_N$  are firing according to a poisson process with an average firing rate  $f_{input}$  when active and with 0 Hz when in an inactive state. The input neurons receive binary input, which is either a black, or a white pixel of an image. Each spike an input neuron generates was modelled by a double exponential

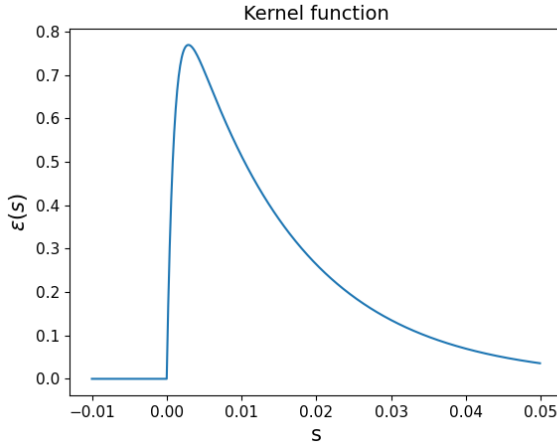


Figure 3.3: Visualization of the kernel function  $\varepsilon(s)$  within the relevant time window. A double exponential kernel was used. To limit the kernel function to positive values of  $s$  a Heaviside step function was applied. The output of this function was used to calculate the unweighed membrane potential response.

kernel. As the signal is zero before the spike is generated, a Heaviside step function  $\theta$  was applied to it, to limit the kernel to time ranges after the spike occurred. The Heaviside step function is given by

$$\theta(s) = \begin{cases} 1 & \text{if } s \geq 0 \\ 0 & \text{if } s < 0 \end{cases}, \quad (3.4)$$

where  $s$  represents a time difference between the current simulation time and the time at which a spike occurred. Multiplying  $\theta(s)$  with the double exponential kernel yields the kernel function

$$\varepsilon(s) = \theta(s) \cdot e^{-(s+\delta t)/\tau_{decay}} - e^{-(s+\delta t)/\tau_{rise}}. \quad (3.5)$$

The kernel function has a time constant for the rise of the signal  $\tau_{rise} = 1ms$  and a time constant for the decay of the signal  $\tau_{decay} = 15ms$ . The time step size of the simulation is  $\delta t = 1ms$ . It had to be added to the double exponential kernel for numerical reasons, to evaluate the time at the end of the current simulation step, rather than at the beginning. A visualization of the kernel function can be seen in Figure 3.3.

### 3 Theoretical background

---

Several input neuron spikes can happen in a short time window, increasing the unweighted membrane potential response  $x_i(t)$ . Depending on the timing of the spikes, they contribute additively to  $x_i(t)$ . The unweighted membrane potential response is given by

$$x_i(t) = \sum_{t_i^{(f)}} \varepsilon(t - t_i^{(f)}), \quad (3.6)$$

with  $t$  being the current simulation time and  $t_i^{(f)}$  the time at which the input spike occurred. Analogously, the unweighted membrane potential response of the prior neurons is given by

$$z_j(t) = \sum_{t_p^{(f)}} \varepsilon(t - t_p^{(f)}), \quad (3.7)$$

The membrane potential  $u_k$  of each output neuron is calculated by multiplying the unweighted membrane potential response of each input neuron times the input weight  $w_{ki}^I$  of the connection between them, plus the unweighted membrane potential response of each prior neuron times the prior weight  $w_{kj}^P$

$$u_k(t) = \sum_{i=1}^N w_{ki}^I \cdot x_i(t) + \sum_{j=1}^J w_{kj}^P \cdot z_j(t). \quad (3.8)$$

In Nessler et al. (2013) each output neuron  $y_k$  also had an intrinsic excitability  $w_{k0}$ , which was learned for each neuron. For the experiments of this thesis it was omitted, as the different classes of input images were equally likely, thus the intrinsic excitabilities of the output neurons would all end up being equal to each other.

Nessler et al. (2013) defined that the firing probability of an output neuron  $y_k$  is exponentially proportional to its membrane potential  $u_k$  minus the received inhibition  $I(t)$

$$p(y_k \text{ fires at time } t) \propto e^{u_k(t) - I(t)}. \quad (3.9)$$

### 3.3 Network model

---

This stochastic firing model is supported by experimental biological evidence (Jolivet et al., 2006). Through this definition the firing rate  $r_k(t)$  of an output neuron is then modelled by an inhomogeneous Poisson process as

$$r_k(t) = e^{u_k(t) - I(t)}. \quad (3.10)$$

At every timestep of the simulation the inhibition signal  $I(t)$  is subtracted from the membrane potential  $u_k(t)$  of every output neuron. By that, the membrane potentials are altered to always yield a spiking frequency of 200 Hz, regardless if it would be lower or higher without it. This means that the adaptive inhibition signal can also function as an excitatory signal.

The total firing rate of the output neurons  $R(t)$  is obtained by summing up the firing rates of all output neurons, yielding

$$R(t) = \sum_{k=1}^K e^{u_k(t) - I(t)}. \quad (3.11)$$

The inhibition signal  $I(t)$  was chosen to depend on the current membrane potential of the output neurons. Solving Equation 3.11 for  $I(t)$  yields

$$R(t) = \frac{\sum_{k=1}^K e^{u_k(t)}}{e^{I(t)}} \quad (3.12)$$

$$e^{I(t)} = \frac{\sum_{k=1}^K e^{u_k(t)}}{R(t)} \quad (3.13)$$

$$I(t) = \ln \frac{\sum_{k=1}^K e^{u_k(t)}}{R(t)} \quad (3.14)$$

$$I(t) = -\ln R(t) + \ln \sum_{k=1}^K e^{u_k(t)}. \quad (3.15)$$

The probability of an individual output neuron to fire within a time step  $\delta t$  is given by

$$r_k(t)\delta t. \quad (3.16)$$

### 3 Theoretical background

---

The conditional probability  $q_k(t)$  that a spike originated from the output neuron  $y_k$  is given by

$$q_k(t) = \frac{r_k(t)\delta t}{R(t)\delta t} = \frac{e^{u_k(t)-I(t)}}{\sum_{k'=1}^K e^{u_{k'}(t)-I(t)}} = \frac{e^{u_k(t)}}{\sum_{k'=1}^K e^{u_{k'}(t)}}. \quad (3.17)$$

The inhibition term cancels out because all output neurons receive the same inhibition, meaning that it is independent of  $k$ . Whenever an output spike should be generated within a time step, according to Equation 3.16, it is determined via the discrete probability distribution  $q_k(t)$  from which  $y_k$  the spike originates. As  $R(t)$  has a fixed value of 200 Hz, which is ensured by  $I(t)$ , it is unlikely that another output spike is generated shortly after the first one. This means, that the output spike generation functions as a soft-WTA function.

**Spike timing dependent plasticity** The input weights  $w_{ki}^I$  between neurons  $x_i$  and  $y_k$  are updated whenever an output neuron fires.  $\sigma$  determines the time window, after which spikes are no longer considered. If  $y_k$  produces a spike, all its weights to the input neurons are updated as

$$\Delta w_{ki}^I = \begin{cases} \lambda \cdot (ce^{-w_{ki}^I} - 1) & \text{if } x_i \text{ fired in } [t^f - \sigma, t^f] \\ \lambda \cdot (-1) & \text{if } x_i \text{ did not fire in } [t^f - \sigma, t^f], \end{cases} \quad (3.18)$$

where  $\lambda$  is the learning rate, the hyperparameter  $c$  shifts the weight values,  $t^f$  is the time when  $y_k$  spiked and  $\sigma$  is the time window in which input spikes are considered as "before" an output spike. As the membrane potentials  $u_k$  of the output neurons result from the addition of the EPSPs of the input neurons times the corresponding weight, a way to control the average size of  $u$  is needed. If  $u$  is too small, the output neurons will fire too sparsely and if  $u$  is too big, it will impair the learning process. So to limit  $u$ , the size of the weights is controlled via the hyperparameter  $c$ . The learning rate  $\lambda$  is needed to control the size of each weight update. If it is too big, few output neurons will respond to too large parts of the input, while others might not respond at all. On the other hand if  $\lambda$  is too small the network will learn very slowly and may never converge. The prior weights  $w_{kj}^P$  are

also updated whenever an output neuron fires, in the same way as  $w_{ki}^I$

$$\Delta w_{kj}^P = \begin{cases} \lambda \cdot (ce^{-w_{kj}^P} - 1) & \text{if } z_j \text{ fired in } [t^f - \sigma, t^f] \\ \lambda \cdot (-1) & \text{if } z_j \text{ did not fire in } [t^f - \sigma, t^f]. \end{cases} \quad (3.19)$$

## 3.4 Mathematical link between the spiking Winner-Take-All network model and Bayesian inference

Nessler et al. (2013) hypothesized that the ensemble of weights of a neuron can be understood as a generative model. They further claimed, that every synaptic weight, due to STDP-induced changes, converges stochastically to the log of the conditional probability that the presynaptic neuron has fired just before the postsynaptic neuron, given that the postsynaptic neuron fires. This connection is given by

$$w_{ki}^I = \log(p(x_i = 1 | y_k = 1)) \quad (3.20)$$

an will be analysed in Section 4.2. Furthermore, they claimed that in a Bayesian inference context, every input spike provides evidence for an observed variable and every output spike represents one stochastic sample from the posterior distribution over hidden causes, which are encoded in the circuit.

To explain the connection between the spiking Winner-Take-All network model and Bayesian inference it will be demonstrated, that the posterior probability of Bayesian inference given in Equation 3.3 is equal to the relative firing probability  $q_k(t)$ , given in Equation 3.17.

As explained in Section 3.2, the visual input, modelled by the input neurons, can be thought of as the Bayesian likelihood  $P(X|Y)$  and the feedback, modelled by the prior neurons, as the Bayesian prior  $P(Y|Z)$ .

It is argued that  $P(X = x|Y = k)$  equals  $q_k^X(t)$ .  $q_k^X(t)$  is the conditional probability of an output neuron  $Y_k$  for the given input vector  $X = x$ . It can be calculated similarly to  $q_k(t)$ , but without the contribution of the prior

### 3 Theoretical background

---

neurons. Thus, the partial membrane potential, caused by the input neurons, is needed and given by

$$u_k^X(t) = \sum_{i=1}^N w_{ki}^I \cdot x_i(t). \quad (3.21)$$

Inserting  $u_k^X(t)$ , instead of  $u_k(t)$  into Equation 3.17 yields

$$q_k^X(t) = \frac{e^{u_k^X(t)}}{\sum_{k'=1}^K e^{u_{k'}^X(t)}} = P(X = x | Y = k). \quad (3.22)$$

Similarly, it is argued that  $P(Y = k | Z = j)$  equals  $q_k^Z(t)$ .  $q_k^Z(t)$  is the conditional probability of an output neuron  $y_k$ , given the activity of a prior neuron  $z_j$ . Analogously to  $u_k^X(t)$ , the partial membrane potential, caused by the prior neurons, is given by

$$u_k^Z(t) = \sum_{j=1}^J w_{kj}^P \cdot z_j(t). \quad (3.23)$$

Inserting  $u_k^Z(t)$ , instead of  $u_k(t)$ , into Equation 3.17 yields

$$q_k^Z(t) = \frac{e^{u_k^Z(t)}}{\sum_{k'=1}^K e^{u_{k'}^Z(t)}} = P(Y = k | Z = j). \quad (3.24)$$

When inserting the likelihood and the prior into Equation 3.3 we get

$$\begin{aligned} P(Y = k | X = x, Z = j) &= \frac{e^{u_k^X(t)} \cdot e^{u_k^Z(t)}}{\sum_{k'=1}^K e^{u_{k'}^X(t)} \cdot e^{u_{k'}^Z(t)}} \\ &= \frac{e^{\sum_{i=1}^N w_{ki}^I \cdot x_i(t)} \cdot e^{\sum_{j=1}^J w_{kj}^P \cdot z_j(t)}}{\sum_{k'=1}^K e^{\sum_{i=1}^N w_{k'i}^I \cdot x_i(t)} \cdot e^{\sum_{j=1}^J w_{k'j}^P \cdot z_j(t)}} \\ &= \frac{e^{\sum_{i=1}^N w_{ki}^I \cdot x_i(t) + \sum_{j=1}^J w_{kj}^P \cdot z_j(t)}}{\sum_{k'=1}^K e^{\sum_{i=1}^N w_{k'i}^I \cdot x_i(t) + \sum_{j=1}^J w_{k'j}^P \cdot z_j(t)}} \end{aligned} \quad (3.25)$$

### 3.4 Mathematical link between the spiking Winner-Take-All network model and Bayesian inference

---

According to Equation 3.17 and 3.8

$$\begin{aligned} q_k(t) &= \frac{e^{u_k(t)}}{\sum_{k'=1}^K e^{u_{k'}(t)}} \\ &= \frac{e^{\sum_{i=1}^N w_{ki}^I \cdot x_i(t) + \sum_{j=1}^J w_{kj}^P \cdot z_j(t)}}{\sum_{k'=1}^K e^{\sum_{i=1}^N w_{k'i}^I \cdot x_i(t) + \sum_{j=1}^J w_{k'j}^P \cdot z_j(t)}}. \end{aligned} \quad (3.26)$$

From Equations 3.25 and 3.26 we can conclude that

$$P(Y = k | X = x, Z = j) = q_k(t). \quad (3.27)$$

This showed, that the Bayesian posterior is equal to the conditional probability  $q_k(t)$ . Furthermore, it showed that the extension of  $u_k(t)$ , in Equation 3.8, with the prior term was correct.



# 4 Experiments

## 4.1 Experiment 1: Horizontal and vertical bars

### 4.1.1 Introduction

For this experiment images of either horizontal or vertical bars were shown to the WTA network. The network trained its weights through unsupervised learning. Through that, it learned to cluster the images together, depending on the orientation and position of the bars. The learning of the network was visualized and analysed. Further, the effect of the prior neurons was demonstrated. Ambiguous images, which showed a horizontal and a vertical bar at the same time, were generated and given to the network. Through that, the network's capability to shift its attention to specific parts of the image, depending on the prior was demonstrated.

### 4.1.2 Methods

**Input data** Black bars, with a width of seven pixels, were drawn onto a white background, with a size of  $35 \times 35$  pixels. The bars could be oriented either horizontally or vertically and be shifted in position. The network was supposed to identify ten different groups within these images, five with a horizontal orientation and five with a vertical orientation. With a chosen bar width of seven pixels the image height and width were determined as 35 pixels, as five bars should have place next to each other, without overlap, in each orientation. Each of those bars represented one group of bars. Thus, each group had a size of seven pixels. Starting to count from position 0, the centers of the groups should be at positions 3, 10, 17, 24, 31. The orientation

## 4 Experiments

---

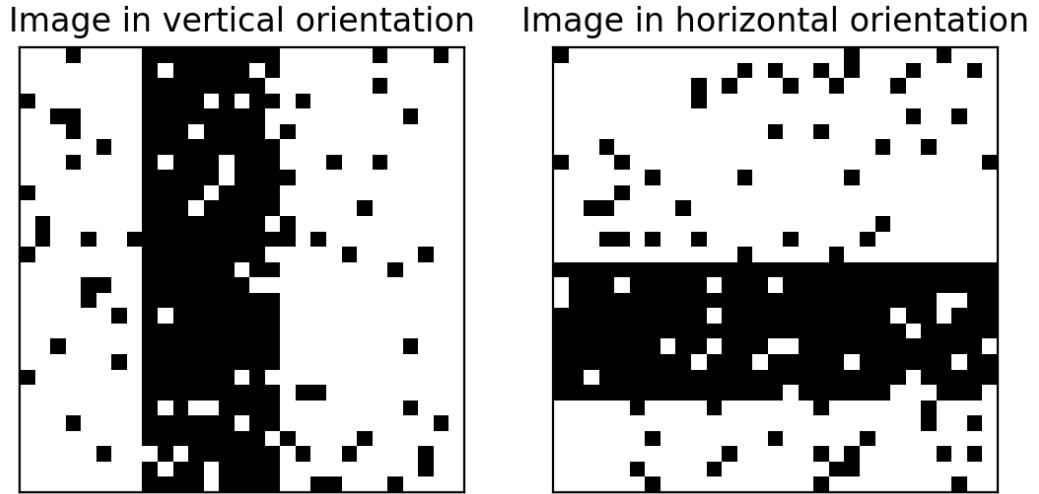


Figure 4.1: Generated training images. One image of each possible orientation at a random position.

of the training images was chosen randomly, via a uniform distribution. The positions of the bars in the training images were also distributed randomly, via a uniform distribution, along the 35 pixels of either axis. To simulate noise, each pixel of an image had a chance of ten percent to have its color flipped after the generation. During the training of the network, random images were generated and presented for 200 ms. As the simulation had a duration of 800 seconds this resulted in 4000 images, which were shown to the network. Examples of the input data can be seen in Figure 4.1. To show the value of the added a-priori information, validation images with two bars forming a cross were also generated, seen in Figure 4.2. When shown to the network in the validation process the prior neurons were given the information that a cross is either of horizontal or vertical orientation.

**Network architecture** The network had 2450 input neurons, as every pixel of an image was connected to two input neurons. Each of these neurons had a firing frequency  $f_{input}$  of 20 Hz, when in the active state and 0 Hz otherwise. Then there were ten output neurons, one for each possible group. Lastly, there were two equal sized groups of prior neurons with firing frequencies  $f_{prior}$  of 200 Hz. This firing frequency was assigned a high

## 4.1 Experiment 1: Horizontal and vertical bars

---

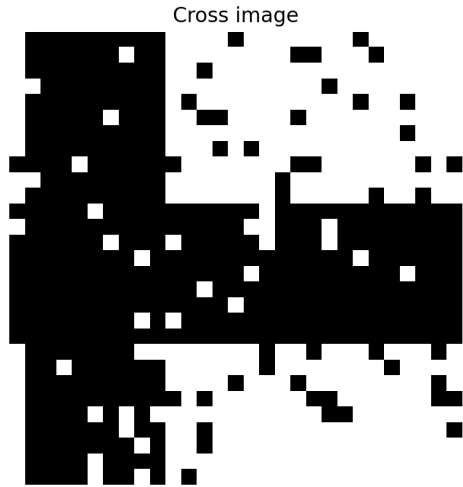


Figure 4.2: Generated cross image, which can represent either horizontal or vertical orientation.

plausible value to keep the needed number of prior neurons small compared to the number of input neurons. During training, the first group  $z^h$  was active when the image was of horizontal orientation and the other group  $z^v$  was active for vertical orientation. Just like the input images' pixels, the prior had a chance of 10 percent to flip. The number of prior neurons had to be determined via grid search, as they needed to be set at values, where the impact of the a-priori information is neither too strong, nor too weak.

**Network and hyperparameters** The simulation of the experiment was performed in time steps of 1 ms. This step size was used for all experiments. As given by Nessler et al. (2013) the time window  $\sigma$  was 10 ms, the time constant for the rise of the EPSPs  $\tau_{rise}$  was 1 ms and the time constant for the decay of the EPSPs  $\tau_{decay}$  was 15 ms. Before performing this experiment, Experiment 2 of Nessler et al. (2013) was reproduced to validate that the implementation of the simulation was correct. This proof of concept was omitted in this work, however, within it the weight shift hyperparameter  $c = 20$  and the learning rate  $\lambda = 10^{-3}$  were determined via grid search. These hyperparameter values were reused for this experiment as the input data, as well as the network architecture, were similar.

### 4.1.3 Results

First, different numbers of prior neurons were tested. Simulations with 10, 20, 50, 100 and 200 prior neurons were performed. For 50, 100 and 200 prior neurons the training process was impaired, by the activity of the prior neurons. Some output neurons were responding to too large areas, while other prior neurons were not responding to any specific areas at all. This happened, for example, because the first output neuron that generated a spike for a horizontal bar got reinforced by the prior neurons to respond to all horizontal bars, no matter the position. Thus, other output neurons were less likely to respond to horizontal bars, resulting in output neurons that were not responding to any specific orientation or area at all. With a number of 10 and 20 prior neurons, each of the output neurons learned to respond to coherent areas of the images. The prior neurons also learned to respond to either horizontal or vertical images. To maximize the impact of the a-priori information the validation of the network was performed with 20 prior neurons, as it was the largest number that resulted in a properly trained network. The results of the training process can be seen in Figure 4.3. In Figure 4.3A examples of input images are shown. The bars were positioned without overlapping each other, thus showing the optimal areas output neurons should learn to respond to. The areas that output neurons did learn to respond to, can be seen in the visualization of the input weights in Figure 4.3B. It can be seen, that the training was successful, as five output neurons responded to horizontal bars and the other five to vertical bars. Furthermore, each output neuron responded to different areas of the input image and there was little overlap between each other. The training progress of the network is given in Figure 4.3E. When the network has completed the training it should mostly have only one or two output neurons being active for any input image. Although, there may be more active output neurons sporadically, due to the stochastic nature of the model. According to this plot, the training process could have been stopped earlier after 2000 shown images. However, as there was no danger of overfitting the data, more images were shown, to ensure that the network had always finished the training when the simulation stopped. In Figure 4.3F the relative activity of the most active output neuron can be seen. First, it can also be used to judge the progress of the training process, as it increased over time. Furthermore,

#### 4.1 Experiment 1: Horizontal and vertical bars

---

it can also be seen as a measure of how clearly an image belonged to the area the most active output neuron responded to. If the position of an image was exactly in the middle of the learned area of the most active output neuron, then the relative activity should be one. However, when the position was on the border between two learned areas of output neurons, then the relative activity should only be 0.5, as the image belonged to both areas. The learned prior weights can be seen in Figure 4.4. There it can be seen, that the first 10 prior neurons learned the same pattern, as all of them were in an active state whenever vertical bars were shown to the network. When comparing these prior weights to the input weights in Figure 4.3B it can be seen that the five highest prior weights of each prior neuron are between themselves and output neurons that learned to respond to vertical bars. The last 10 prior weights showed exactly the opposite pattern, having their five highest weight values between themselves and output neurons that responded to horizontal bars.

To validate the learned patterns, the network was shown horizontal bars with a height of seven pixels, with their centers at every possible position, beginning at position zero and incrementing in steps of one. Each image was shown for 200 ms each, while recording the output neuron activity. To visualize which output neuron is the most active for each position, a horizontal bar with a height of one was drawn into a  $35 \times 35$  pixel image, color-coded to represent the most active output neuron for that position. This can be seen in Figure 4.5A.  $y_7$  and  $y_{10}$  claimed areas with heights of eight pixels, while the areas of  $y_9$  and  $y_4$  had only a height of six pixels. Only  $y_2$  had an area height of the expected seven pixels. These varying heights were expected to happen, due to the stochastic nature of the model and the unsupervised learning method applied in this thesis. Depending on the randomly generated images the network received during the training process, there may be more images on one side of the border between two output neurons, than on the other side. This would result in the favoured neuron having stronger weights around the border area. Because of that, the favoured neuron might end up claiming a larger active area. The output spikes of the network can be seen in Figure 4.5B. It can be seen, that outside of the border areas between the output neurons there was mostly only one neuron active. However, shortly after two seconds  $y_8$  was active. The time frame between 2 seconds and 2.2 seconds corresponds to position 10.  $y_8$

## 4 Experiments

---

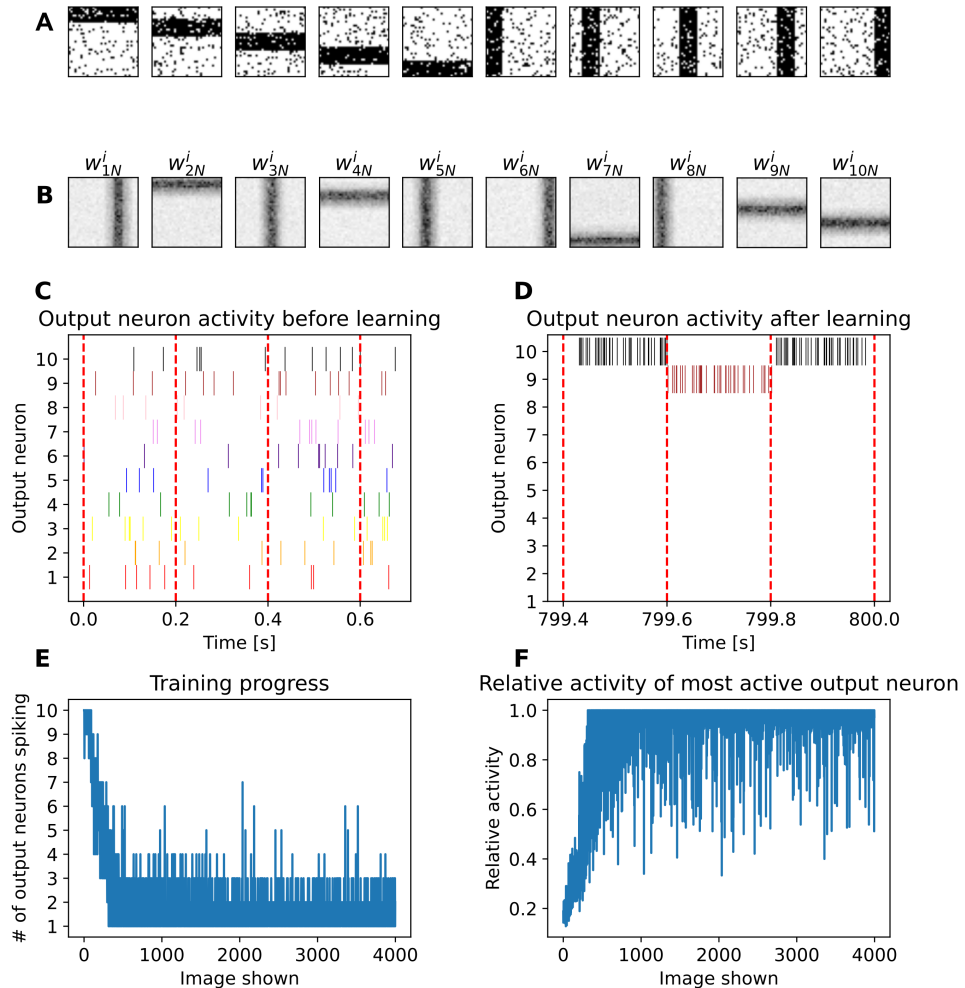


**Figure 4.3: Training with 20 prior neurons.** **A** Examples of  $35 \times 35$ -pixel input images of horizontal and vertical bars with background noise. They were positioned without overlapping each other's bars, thus showing the optimal areas output neurons should learn to respond to. **B** Learned weights of the connections between the input neurons, that were active for black pixels of the input image, and output neurons. As there was one such input neuron per pixel of the image the weights could be plotted in the same format as the image to easily interpret them. **C, D** Spike activity expressed by the output neurons before and after the training of the network. **E** Number of active output neurons during the presentation duration of each training image. **F** This shows the number of spikes the most active output neuron generated, relative to the number of spikes all other output neurons generated combined.

#### 4.1 Experiment 1: Horizontal and vertical bars

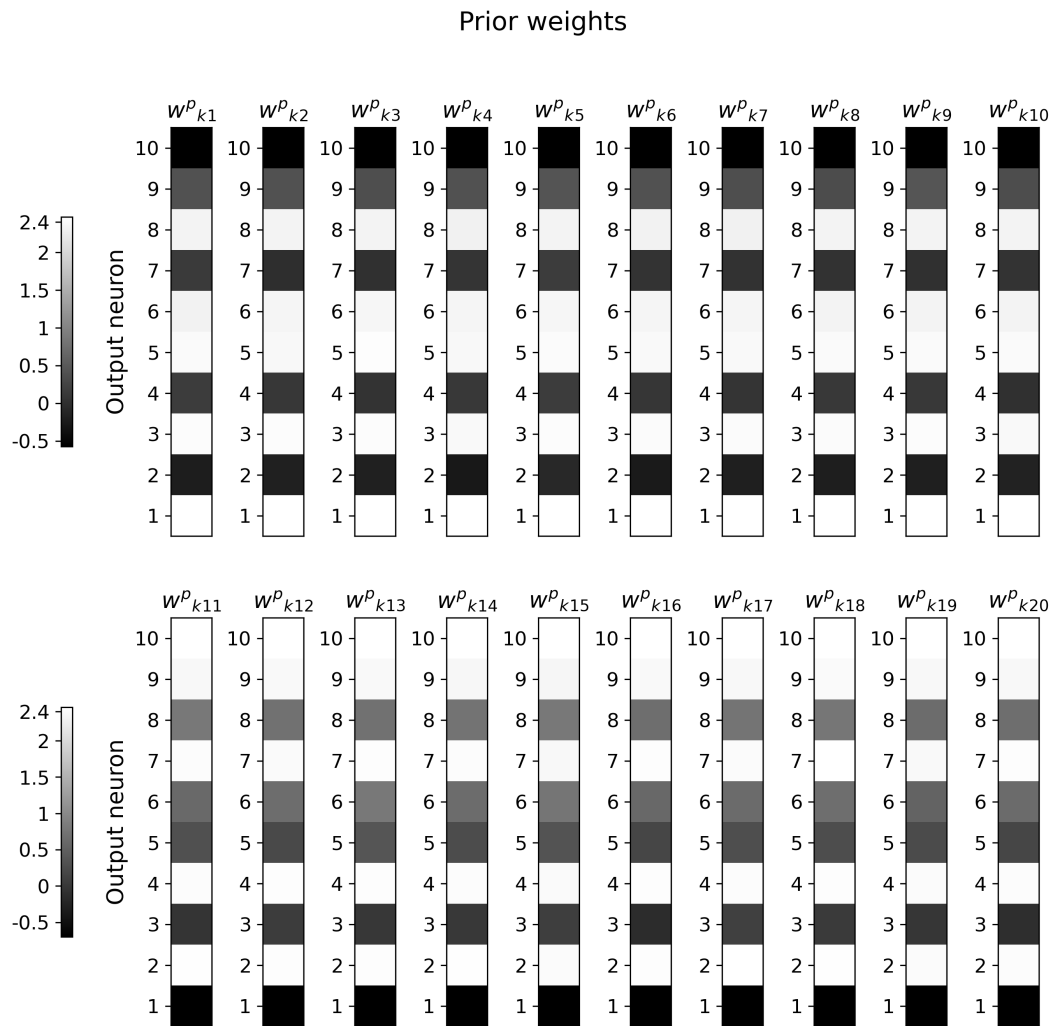


Figure 4.4: Learned weights of the connections between prior and output neurons.

## 4 Experiments

---

should mostly be active for vertical bars, however, its learned area has some overlap with a horizontal bar at position ten and thus there is always a small chance for it to generate a spike. In Figure 4.5C the number of active output neurons for each position is given. The validation process was repeated ten times and the mean and standard deviation of the number were calculated. In this plot four peaks appeared. These peaks are around the borders between the adjacent active areas of output neurons seen in Figure 4.5A. Around the border areas a number of active output neurons bigger than one was expected, as the horizontal bars reach into the areas of two output neurons at once. When looking at the number of active output neurons at position 10, which is approximately 1.1 with a high standard deviation, it shows that  $y_8$  did not falsely learn to be active for horizontal bars, but rather that it was a stochastic outlier. Figure 4.5D shows the relative activity of the most active output neuron. Compared to Figure 4.5C, it provides the additional information of how split the activity of neighbouring output neurons is in the border areas. For example, it can be seen that at position 22  $y_4$  had a relative activity of 0.62. It was only barely able to be the most active neuron and might almost have had only an active area with a height of five pixels.

The validation process for the vertical bars was done analogously to the horizontal bars. Its results are given in Figure 4.6.

Next, the impact of the prior was analysed. An image with a horizontal bar at position 12 and a vertical bar at position 5 on it was generated. First, the prior neurons  $z^v$  were activated and  $z^h$  were deactivated. Then the image was shown to the network for 200 ms. After that the activity of the prior neurons was reversed and the image was shown again. The results can be seen in Figure 4.7. In that figure it can be seen, that the output of the network completely changes, depending of the prior activity. The prior neurons determine if the network focuses on the vertical or horizontal bar of the image.

To further illustrate the dependence of the output on the prior, the firing frequencies of the prior neurons were gradually changed. The starting firing frequency of  $z^h$  was set to 200 Hz and to 0 Hz for  $z^v$ . For those firing frequencies a cross image was shown to the network for 200 ms. It had a horizontal bar at position 31 and a vertical bar at position 3. These position

## 4.1 Experiment 1: Horizontal and vertical bars

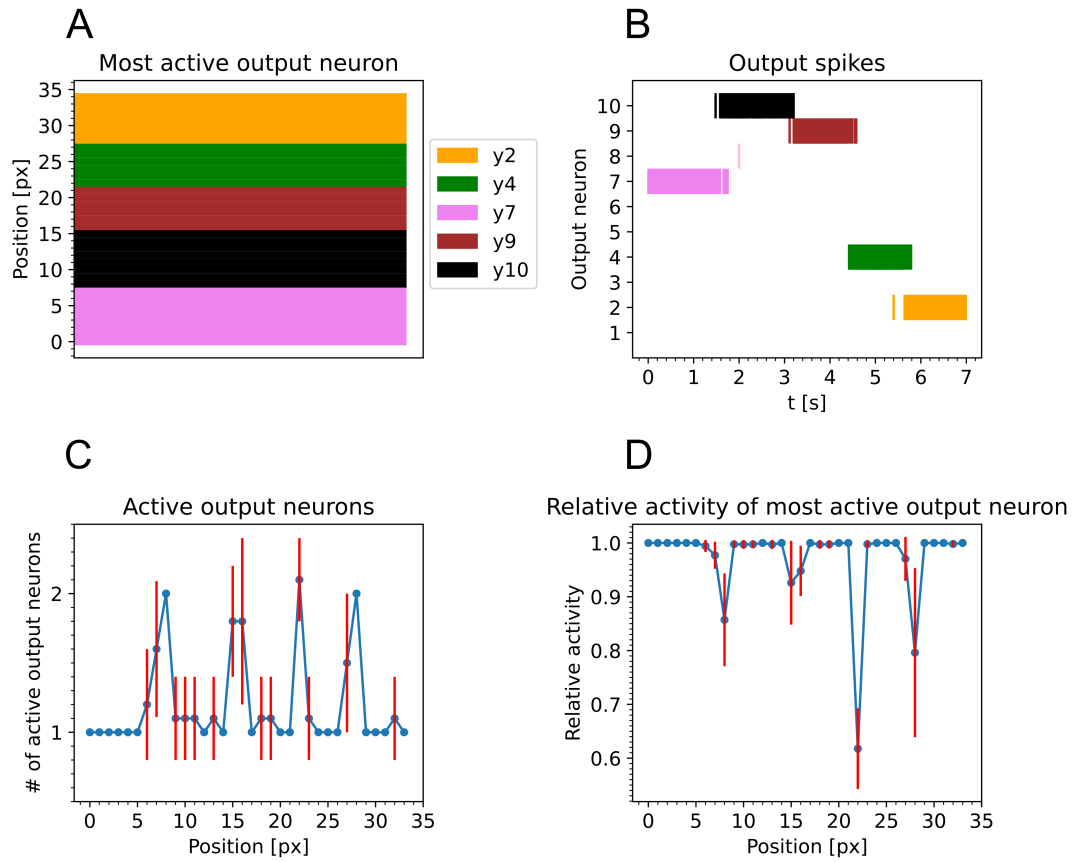


**Figure 4.5: Horizontal validation.** Horizontal bars with a height of seven pixels were shown to the network at different positions. **A** Most active output neuron, depending on the vertical position of the center of a horizontal bar. **B** Output spikes during the validation process. The ticks of the x-axis are in steps of 0.2 seconds, thus each tick signifies the start of a new image being shown. **C** The mean number of active output neurons, depending on the vertical position of a horizontal bar. The standard deviation is given by the red bars. **D** This shows the number of spikes that the most active output neuron generated, relative to the number of spikes all other output neurons generated combined. The blue dots indicate the mean and the red bars the standard deviation.

## 4 Experiments

---

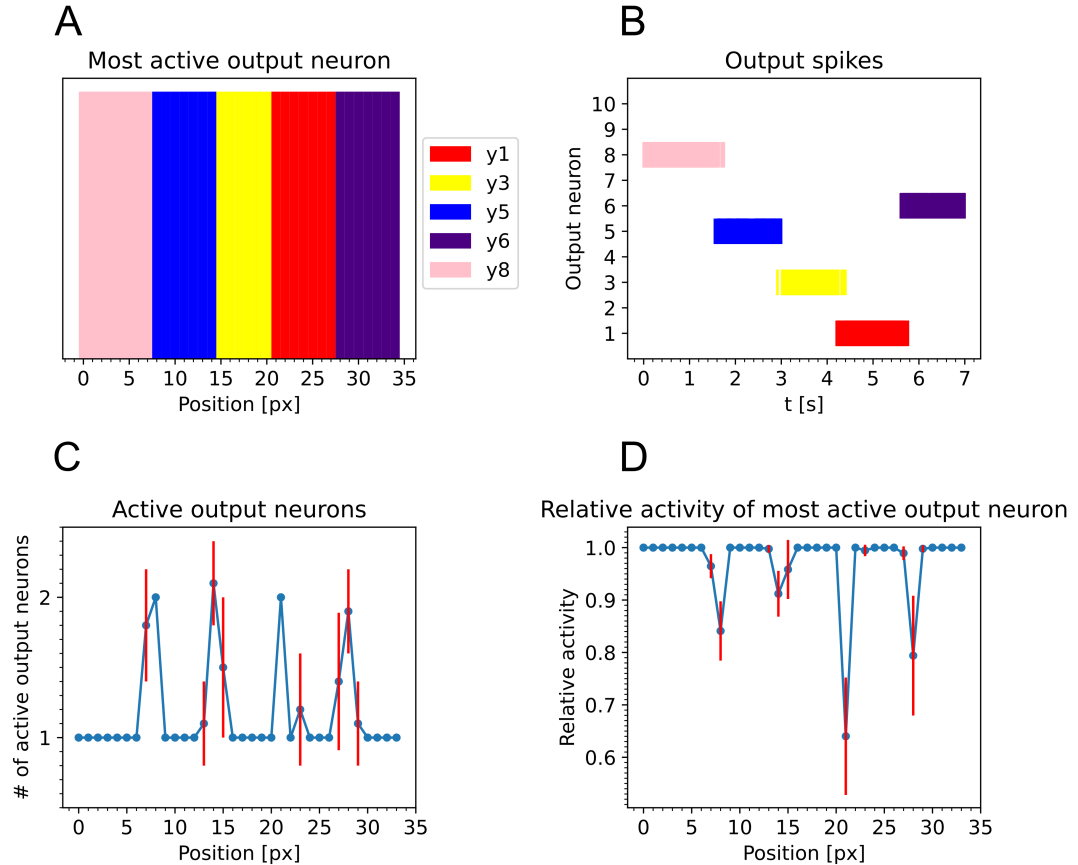


**Figure 4.6: Vertical validation.** Vertical bars with a height of seven pixels were shown to the network at different positions. **A** Most active output neuron, depending on the horizontal position of the center of a vertical bar. **B** Output spikes during the validation process. The ticks of the x-axis are in steps of 0.2 seconds, thus each tick signifies the start of a new image being shown. **C** The mean number of active output neurons, depending on the horizontal position of a vertical bar. The standard deviation is given by the red bars. **D** This shows the number of spikes that the most active output neuron generated, relative to the number of spikes all other output neurons generated combined. The blue dots indicate the mean and the red bars the standard deviation.

#### 4.1 Experiment 1: Horizontal and vertical bars

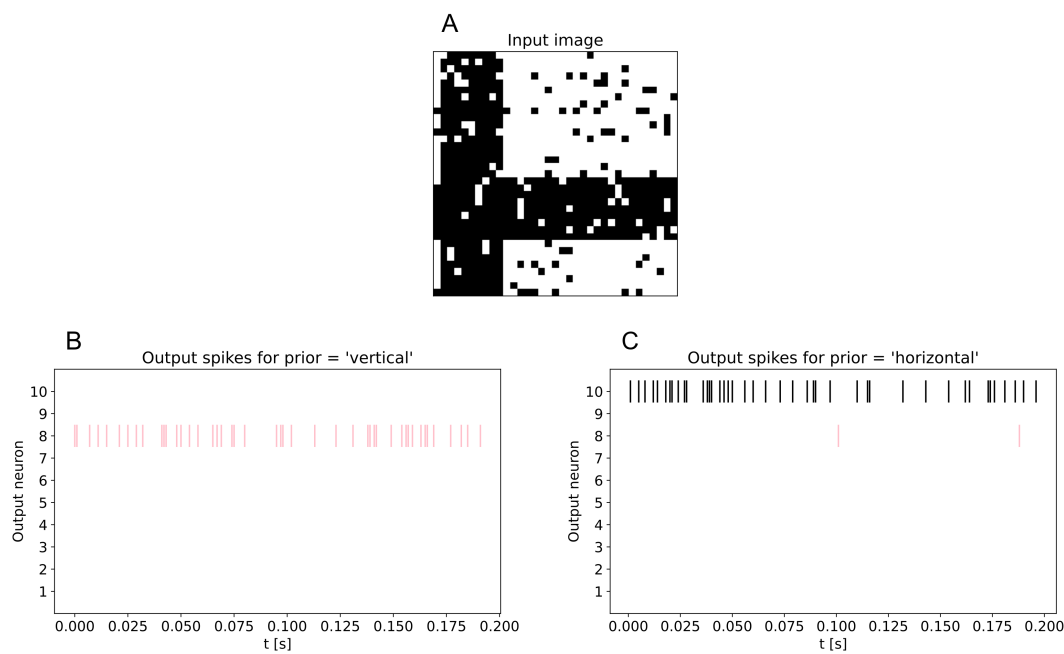


Figure 4.7: Impact of the prior Neurons. **A** Validation image with a horizontal and a vertical bar on it. **B** Spiking activity of the output neurons with  $z^v$  being active. **C** Spiking activity of the output neurons with  $z^h$  being active.

are as far at the edge of the image as possible, while still displaying the whole width of the bars. After each image presentation duration the firing frequency of  $z^h$  was decreased by 1 Hz and increased by 1 Hz for  $z^v$ . The used cross image can be seen in Figure 4.8A. The firing frequency of the 2 most active output neurons, depending on the firing frequency of  $z^v$ , can be seen in Figure 4.8B. At the beginning  $y_2$ , which represents the horizontal part of the cross image, was the most active neuron, which is correct as the prior neurons fully supported the horizontal interpretation of the input image. With rising firing frequency of  $z^v$ , the activity of  $y_2$  decreased and the activity of  $y_8$  increased. This happened, because the prior neurons gradually supported the interpretation of the image as vertical more and more. It was expected, that the crossing point of the two graphs in Figure 4.8B would be at a firing frequency of  $z^v$  of 100 Hz, however, the graphs crossed at 58.6 Hz. In Figure 4.5D the relative activity of  $y_2$  at the edge of the bar, at position 28, was 0.79. In Figure 4.6D the relative activity of  $y_8$  at the edge of the bar, at position 6, was 1.0.  $y_8$  has a higher relative activity at that position than  $y_2$  at position 28, because  $y_8$  has an active area of width 8, making position 6 not the border of the active area. Due to the larger active area of  $y_8$  the crossing point shifted in favour of  $y_8$ .

## 4.2 Experiment 2: Mathematical analysis and simulation of the network with 1-D images

### 4.2.1 Introduction

The purpose of this experiment was to analyse a smaller network and to provide a definitive way to verify the performance of the simulation. Furthermore, the weights were not learned, as in the previous experiment, but rather determined analytically. This was done to experimentally prove the relation, given by Nessler et al. (2013), that the weights stochastically converge toward the conditional probability, that a presynaptic neuron fired shortly before the postsynaptic neuron. First, the network was scaled down to be one-dimensional with 18 input neurons, four prior neurons and four output neurons, making it easier to analyse. The weights were

## 4.2 Experiment 2: Mathematical analysis and simulation of the network with 1-D images

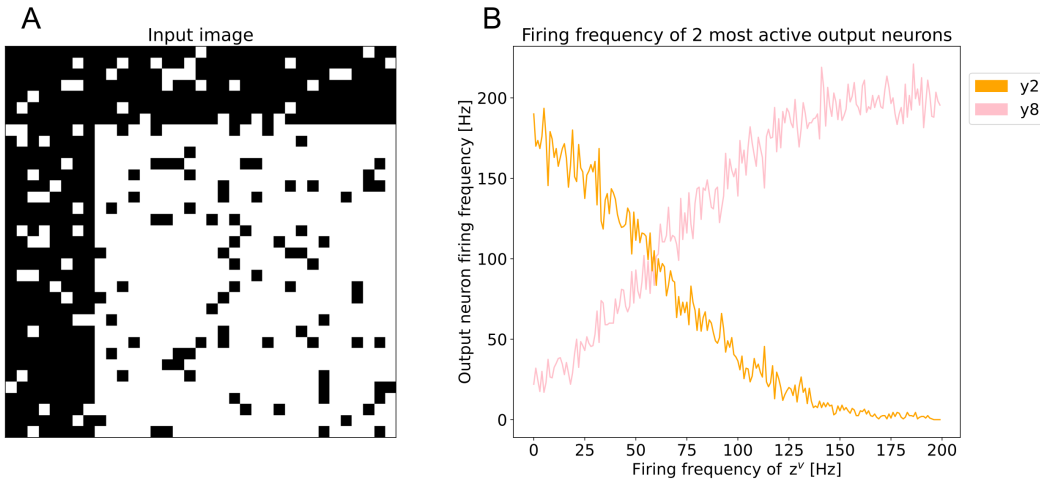


Figure 4.8: **Cross image with varying prior neuron activity.** **A** Validation cross image. **B** Firing frequency of the 2 most active output neurons, depending on the firing frequency of  $z^v$ . The output neuron firing frequencies were averaged over 10 runs to smooth the graphs.

determined by utilizing the logarithmic connection between them and the corresponding conditional probabilities, as given by Equation 3.20. The conditional probabilities of the input and output neurons of the network were calculated and then used to determine the posterior probability of the network. After the simulation of the network, the distribution of the output spikes was used, to calculate the posterior probability. The posterior probabilities, of both the mathematical analysis and the simulation, were compared. It was tuned to approximate the analytical solution as closely as possible, by varying three network hyperparameters.

### 4.2.2 Methods

**Input data** The input image consisted of nine pixels in a horizontal line. Within those nine pixels, going from position 0 to 8, four output classes could be represented. Each output class had three pixels next to each other. This resulted in each output class overlapping its neighbour classes, by one pixel. Thus, the centers of the output classes were at position 1, 3, 5 and 7.

**Network architecture** Only the amount of neurons was changed, compared to the architecture of the previous experiment. As there have to be 2 input neurons for each pixel, one neuron being active if the pixel is white and one if the pixel is black, the network had 18 input neurons. Furthermore, four prior neurons were implemented, of which only one is being active for one of the output classes at a time. Lastly, the network had four output neurons.

**Mathematical Analysis** The posterior probability of the network was calculated by using Equation 3.3.  $P(X = x|Y = k)$  and  $P(Y = k|Z = j)$  were derived, corresponding to the paradigm of the experiment. The calculation of  $P(X = x|Y = k)$  was split into two parts. First, the contribution of the active input neurons was calculated by determining the matrix  $P^{X|Y}$ . This matrix is of size  $4 \times 9$  and contains the conditional probabilities of each input neuron  $y_k$  being active, given that an output neuron  $x_i$  is active. These probabilities were calculated, by determining which input neurons are active depending on the output class and which input neurons are inactive, as dictated by the network architecture. Furthermore, the noise that was applied to the input neurons had to be taken into account. For input neurons, belonging to the output class, the conditional probability was determined as 1 and lowered by the noise level. For the input neurons outside of the 3-wide pixel block, which belongs to the output class, it was determined as 0 and raised by the noise level. According to this  $P^{X|Y}$  is given by

$$P_{k,i}^{X|Y} = \begin{cases} 1 - \text{noise level} & \text{if } x_i \text{ is in the active area of } y_k, \\ 0 + \text{noise level} & \text{if } x_i \text{ is not in the active area of } y_k \end{cases}. \quad (4.1)$$

After calculating all entries of  $P^{X|Y}$  its rows were multiplied with the input image vector

$$P_1(X = x|Y = k) = P_{k,*}^{X|Y} \cdot x \quad (4.2)$$

resulting in a conditional probability that the input vector of the active pixels belongs to output class  $k$ . The input vector was given with entries of 1 for active pixels and with entries of 0 for inactive pixels. Next, to include the contribution of the input neurons that are spiking when a pixel is inactive, the conditional probability of the input neurons that are active for the

## 4.2 Experiment 2: Mathematical analysis and simulation of the network with 1-D images

---

entries, where  $x_i = 0$ , had to be calculated. To achieve this complementary conditional probability at first  $P^{X|Y}$  was subtracted from one. To include the correct conditional probabilities for the complementary case the input image vector  $x$  was then also subtracted from one.  $1 - P^{X|Y}$  and  $1 - x$  were multiplied to yield

$$P_2(X = x|Y = k) = (1 - P_{k,*}^{X|Y}) \cdot (1 - x). \quad (4.3)$$

The results of both calculations were then multiplied element-wise to yield

$$P(X = x|Y = k) = P_1(X = x|Y = k) \odot P_2(X = x|Y = k). \quad (4.4)$$

$P(Y = k|Z = j)$  was determined by first calculating the matrix  $P^{Y|Z}$ . It has a dimension of  $4 \times 4$  and contains the conditional probabilities for the output neuron  $y_k$ , given the prior neuron  $z_j$  being active. For each output class, there exists one corresponding prior neuron. As there can never be more than one active prior neuron at a time,  $P^{Y|Z}$  is given by

$$P_{k,j}^{Y|Z} = \begin{cases} 1 - \text{noise level} & \text{if } i = j, \\ 0 + \frac{1}{3} \text{noise level} & \text{if } i \neq j. \end{cases} \quad (4.5)$$

$P(Y = k|Z = j)$  was then obtained by

$$P(Y = k|Z = j) = P^{Y|Z} \cdot z, \quad (4.6)$$

where  $z$  is given by a  $4 \times 1$  one-hot encoded vector of the prior. Finally, inserting  $P(X = x|Y = k)$  and  $P(Y = k|Z = j)$  into Equation 3.3 yields the analytical posterior  $P_{\text{analysis}}(Y = k|X = x, Z = j)$ .

**Simulation** The input weights for the simulation were calculated as two separate sets. First, weights  $w^{I1}$  for the input neurons that are active for active input pixels were determined by

$$w^{I1} = \ln(P^{X|Y}). \quad (4.7)$$

Then, complementary input weights  $w^{I2}$  were calculated for input neurons representing non active input pixels with

$$w^{I2} = \ln(1 - P^{X|Y}). \quad (4.8)$$

## 4 Experiments

---

The prior weights  $w^P$  were derived by

$$w^P = \ln(P^{Y|Z}). \quad (4.9)$$

The network was simulated for six different input images for each hyperparameter set. These six images were hand-picked, to include specific edge cases and to allow comparability of the results of different hyperparameter sets. After the image presentation period of each input image, the numbers of output spikes of each class were counted and their proportions were calculated to yield the posterior  $P_{simulation}(Y = k|X, Z)$ . The Kullback-Leibler divergence was chosen, to compare the divergence of the analytic and the simulated posteriors of the network. This divergence is a type of statistical distance and indicates how much two probability distributions diverge from each other. In the context of Bayesian inference it gives the amount of information lost, when  $P_{simulation}(Y = k|X, Z)$  is used to approximate  $P_{analysis}(Y = k|X, Z)$ . The goal of the hyperparameter search of the simulation, was to minimize the Kullback-Leibler divergence. After showing an output image to the network, the Kullback-Leibler divergence was calculated as

$$\begin{aligned} D_{KL}(P_{analysis}(Y = k|X, Z) || P_{simulation}(Y = k|X, Z)) = \\ \sum_{k=1}^K P_{analysis}(Y = k|X, Z) \cdot \ln\left(\frac{P_{analysis}(Y = k|X, Z)}{P_{simulation}(Y = k|X, Z)}\right), \end{aligned} \quad (4.10)$$

where  $K$  is the number of output neurons and  $P_{analysis}(Y = k|X, Z)$  and  $P_{simulation}(Y = k|X, Z)$  are the posteriors of the network, later called "analysis output probabilities" and "simulation output probabilities" in plots. The six resulting Kullback-Leibler divergences for each hyperparameter set were averaged, to create a single metric, by which the performance of the different hyperparameter sets was compared. The three hyperparameters input firing rate  $f_{input}$ , prior firing rate  $f_{prior}$  and the membrane constant  $\tau_{decay}$  were varied, to inspect their influence on the result, as well as to approximate the analytical solution as closely as possible. Each input image was presented to the network for 20 seconds, to reduce the variance between runs. Furthermore, each simulation was repeated 20 times, with the same hyperparameter set, to obtain the mean and standard deviation of the simulation output probabilities and of the Kullback-Leibler divergence.

### 4.2.3 Results

**Analytic Results** First, the matrix  $P^{X|Y}$  was calculated using Equation 4.1

$$P^{X|Y} = \begin{bmatrix} 0.9 & 0.9 & 0.9 & 0.1 & 0.1 & 0.1 & 0.1 & 0.1 & 0.1 \\ 0.1 & 0.1 & 0.9 & 0.9 & 0.9 & 0.1 & 0.1 & 0.1 & 0.1 \\ 0.1 & 0.1 & 0.1 & 0.1 & 0.9 & 0.9 & 0.9 & 0.1 & 0.1 \\ 0.1 & 0.1 & 0.1 & 0.1 & 0.1 & 0.1 & 0.9 & 0.9 & 0.9 \end{bmatrix}. \quad (4.11)$$

Next, the matrix  $P^{Y|Z}$  was calculated using Equation 4.5

$$P^{Y|Z} = \begin{bmatrix} 0.9 & 0.0333 & 0.0333 & 0.0333 \\ 0.0333 & 0.9 & 0.0333 & 0.0333 \\ 0.0333 & 0.0333 & 0.9 & 0.0333 \\ 0.0333 & 0.0333 & 0.0333 & 0.9 \end{bmatrix}. \quad (4.12)$$

**Simulation results with prior disabled** The network was at first simulated with inactive prior neurons, to simplify the hyperparameter fitting process. The prior neurons were reactivated and  $f_{prior}$  was fitted, after determining the best values for  $f_{input}$  and  $\tau_{decay}$ . The values 0.015 seconds and 0.004 seconds for  $\tau_{decay}$  were used for the simulation and compared. For each of these values, an optimal value for  $f_{input}$  was found, by looking for the value that yielded the smallest Kullback-Leibler divergence.

$\tau_{decay} = 0.015\text{seconds}$ ,  $f_{prior} = 0\text{Hz}$  Values for  $f_{input}$  between 10 and 110 Hz in steps of 10 Hz were simulated. After identifying the input firing rate with the smallest Kullback-Leibler divergence, the network was simulated again for  $f_{input}$  values  $\pm 10$  Hz in steps of 2 Hz. The result of this search can be seen in Figure 4.9. This process yielded the best input firing rate of 42 Hz. The results of this hyperparameter combination can be seen in Figure 4.10. In this figure six different input images can be seen in A. The active pixels are shown in black. In B the posterior probabilities of the mathematical analysis are given by the red bars and the posterior probabilities of the simulation are given by the blue bars. Each simulation output probability has its standard deviation marked by a black bar. At the bottom the value

## 4 Experiments

---

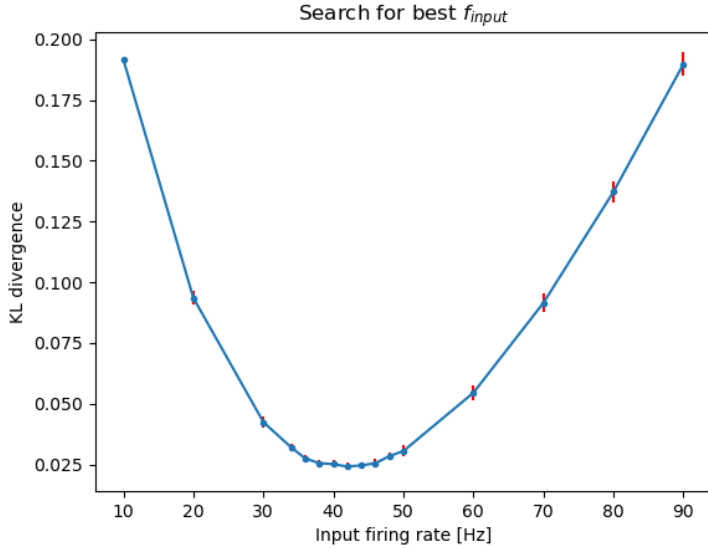
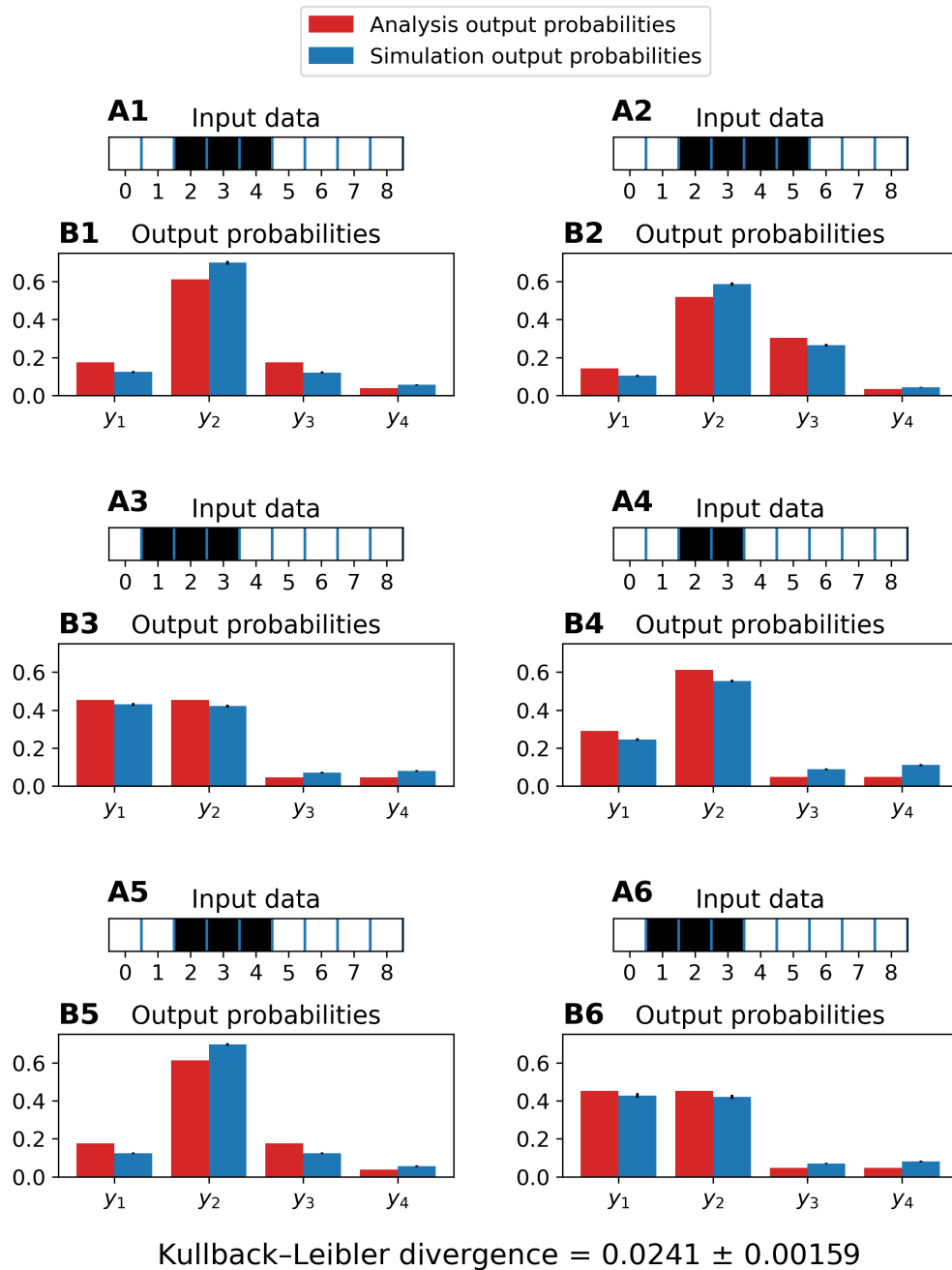


Figure 4.9: KL divergence for different  $f_{input}$  values. Hyperparameters:  $f_{prior} = 0\text{Hz}$ ,  $\tau_{decay} = 15\text{ms}$

	Image 1		Image 2	
	Analysis	Simulation	Analysis	Simulation
$y_0$	0.175	$0.124 \pm 0.0061$	0.143	$0.104 \pm 0.0059$
$y_1$	0.612	$0.699 \pm 0.0093$	0.518	$0.587 \pm 0.0090$
$y_2$	0.175	$0.121 \pm 0.0058$	0.304	$0.266 \pm 0.0067$
$y_3$	0.038	$0.056 \pm 0.0033$	0.035	$0.043 \pm 0.0025$
	Image 3		Image 4	
$y_0$	0.453	$0.430 \pm 0.0089$	0.291	$0.245 \pm 0.0065$
$y_1$	0.453	$0.421 \pm 0.0073$	0.613	$0.553 \pm 0.0072$
$y_2$	0.047	$0.070 \pm 0.0045$	0.048	$0.090 \pm 0.0045$
$y_3$	0.047	$0.080 \pm 0.0042$	0.048	$0.111 \pm 0.0053$
	Image 5		Image 6	
$y_0$	0.175	$0.124 \pm 0.0046$	0.453	$0.428 \pm 0.0116$
$y_1$	0.612	$0.697 \pm 0.0069$	0.453	$0.421 \pm 0.0111$
$y_2$	0.175	$0.123 \pm 0.0050$	0.047	$0.070 \pm 0.0034$
$y_3$	0.038	$0.056 \pm 0.0043$	0.047	$0.081 \pm 0.0047$

Table 4.1: Analysis and simulation output probabilities. Hyperparameters:  $f_{input} = 42\text{Hz}$ ,  $f_{prior} = 0\text{Hz}$ ,  $\tau_{decay} = 15\text{ms}$

## 4.2 Experiment 2: Mathematical analysis and simulation of the network with 1-D images



**Figure 4.10: Analysis and simulation result.** Hyperparameters:  $f_{input} = 42\text{Hz}$ ,  $f_{prior} = 0\text{Hz}$ ,  $\tau_{decay} = 15\text{ms}$ . **A** Input images with  $9 \times 1$  pixels, active pixels in black. **B** Analytically calculated posterior probabilities and simulated posterior probabilities. The standard deviations are given by the black bars.

## 4 Experiments

---

	Image 1		Image 2	
	Analysis	Simulation	Analysis	Simulation
$y_0$	0.175	$0.061 \pm 0.0038$	0.143	$0.049 \pm 0.0027$
$y_1$	0.612	$0.861 \pm 0.0065$	0.518	$0.715 \pm 0.0083$
$y_2$	0.175	$0.061 \pm 0.0041$	0.304	$0.226 \pm 0.0070$
$y_3$	0.038	$0.017 \pm 0.0016$	0.035	$0.011 \pm 0.0017$
	Image 3		Image 4	
$y_0$	0.453	$0.472 \pm 0.0100$	0.291	$0.207 \pm 0.0067$
$y_1$	0.453	$0.464 \pm 0.0101$	0.613	$0.685 \pm 0.0080$
$y_2$	0.047	$0.027 \pm 0.0027$	0.048	$0.043 \pm 0.0037$
$y_3$	0.047	$0.037 \pm 0.0032$	0.048	$0.065 \pm 0.0042$
	Image 5		Image 6	
$y_0$	0.175	$0.061 \pm 0.0033$	0.453	$0.475 \pm 0.0086$
$y_1$	0.612	$0.864 \pm 0.0062$	0.453	$0.459 \pm 0.0087$
$y_2$	0.175	$0.057 \pm 0.0036$	0.047	$0.028 \pm 0.0018$
$y_3$	0.038	$0.018 \pm 0.0022$	0.047	$0.038 \pm 0.0032$

Table 4.2: **Analysis and simulation output probabilities.** Hyperparameters:  $f_{input} = 70\text{Hz}$ ,  $f_{prior} = 0\text{Hz}$ ,  $\tau_{decay} = 15\text{ms}$

of the Kullback-Leibler divergence is given, with its standard deviation. The exact numeric probabilities are given in Table 4.1.

When  $f_{input}$  was 70 Hz the results of the analysis and the simulation differed more as can be seen in Figure 4.11 and Table 4.2.

$\tau_{decay} = 0.004\text{seconds}$ ,  $f_{prior} = 0\text{Hz}$  For this hyperparameter combination values between 50 and 150 Hz for  $f_{input}$  in steps of 10 Hz were simulated. Analogously to the previous hyperparameter set, after finding the best input firing rate, the search was performed in finer steps, until the best value was found at 88 Hz. The result of this search can be seen in Figure 4.12. The result of the simulation, with those hyperparameters, can be seen in Figure 4.13 and Table 4.3.

**Simulation results with prior enabled** After determining the best input firing rates for two different values of  $\tau_{decay}$ , the prior neurons were activated

## 4.2 Experiment 2: Mathematical analysis and simulation of the network with 1-D images

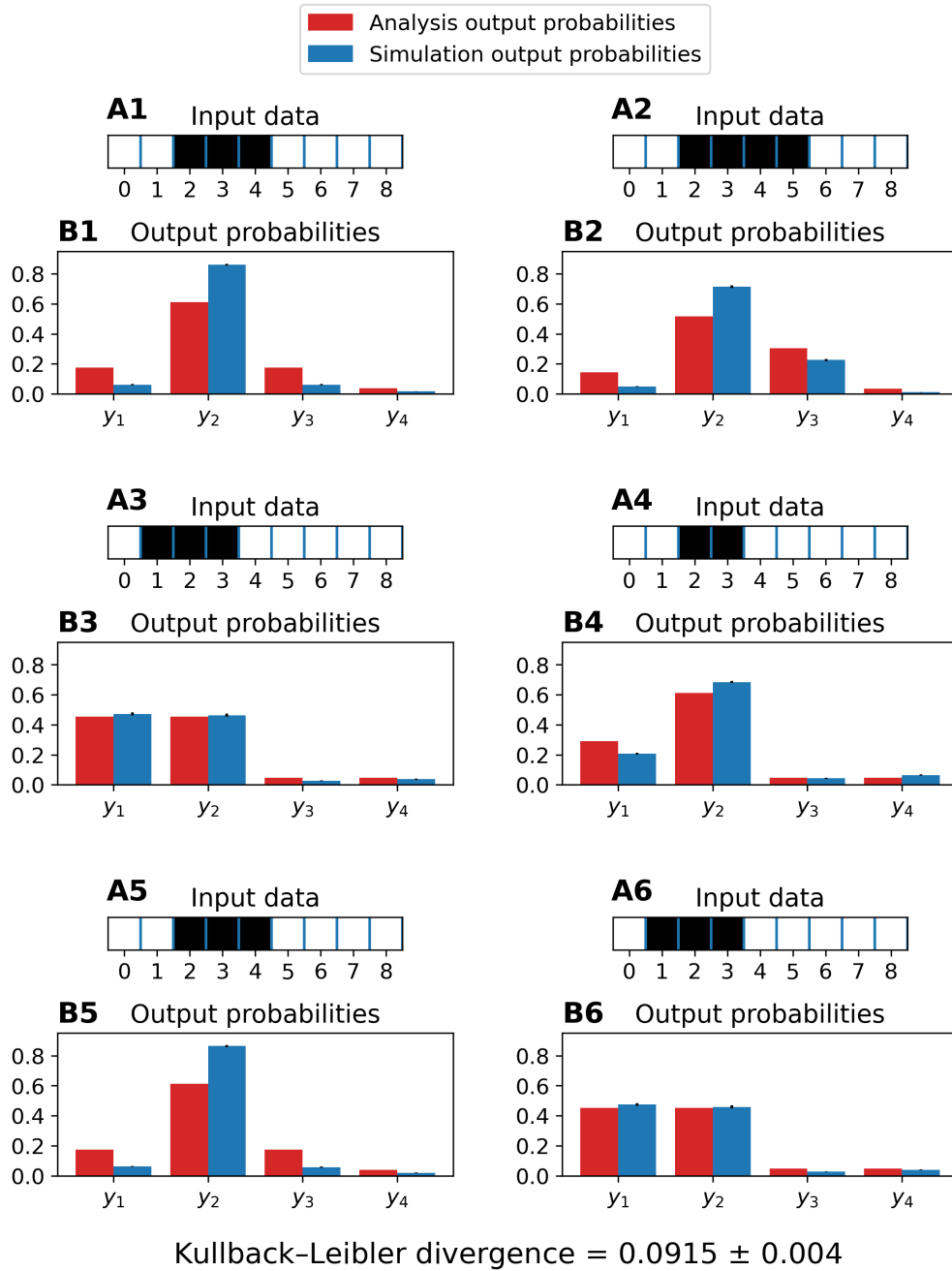


**Figure 4.11: Analysis and simulation result.** Hyperparameters:  $f_{input} = 70Hz$ ,  $f_{prior} = 0Hz$ ,  $\tau_{decay} = 15ms$  **A** Input images with  $9 \times 1$  pixels, active pixels in black. **B** Analytically calculated posterior probabilities and simulated posterior probabilities. The standard deviations are given by the black bars.

## 4 Experiments

---

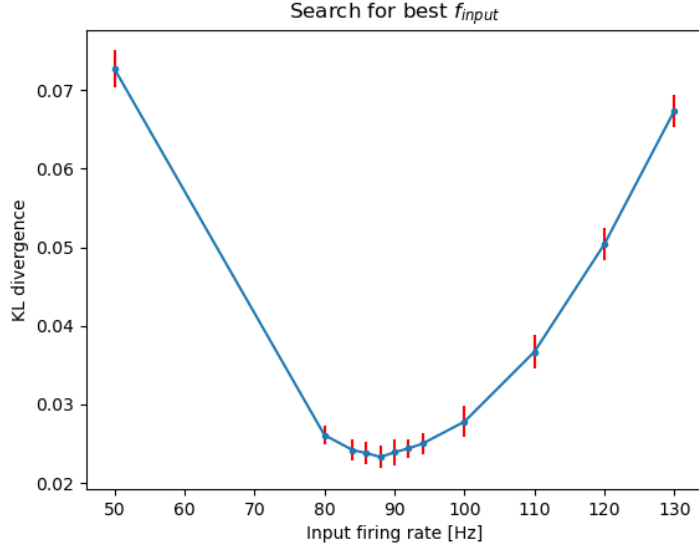
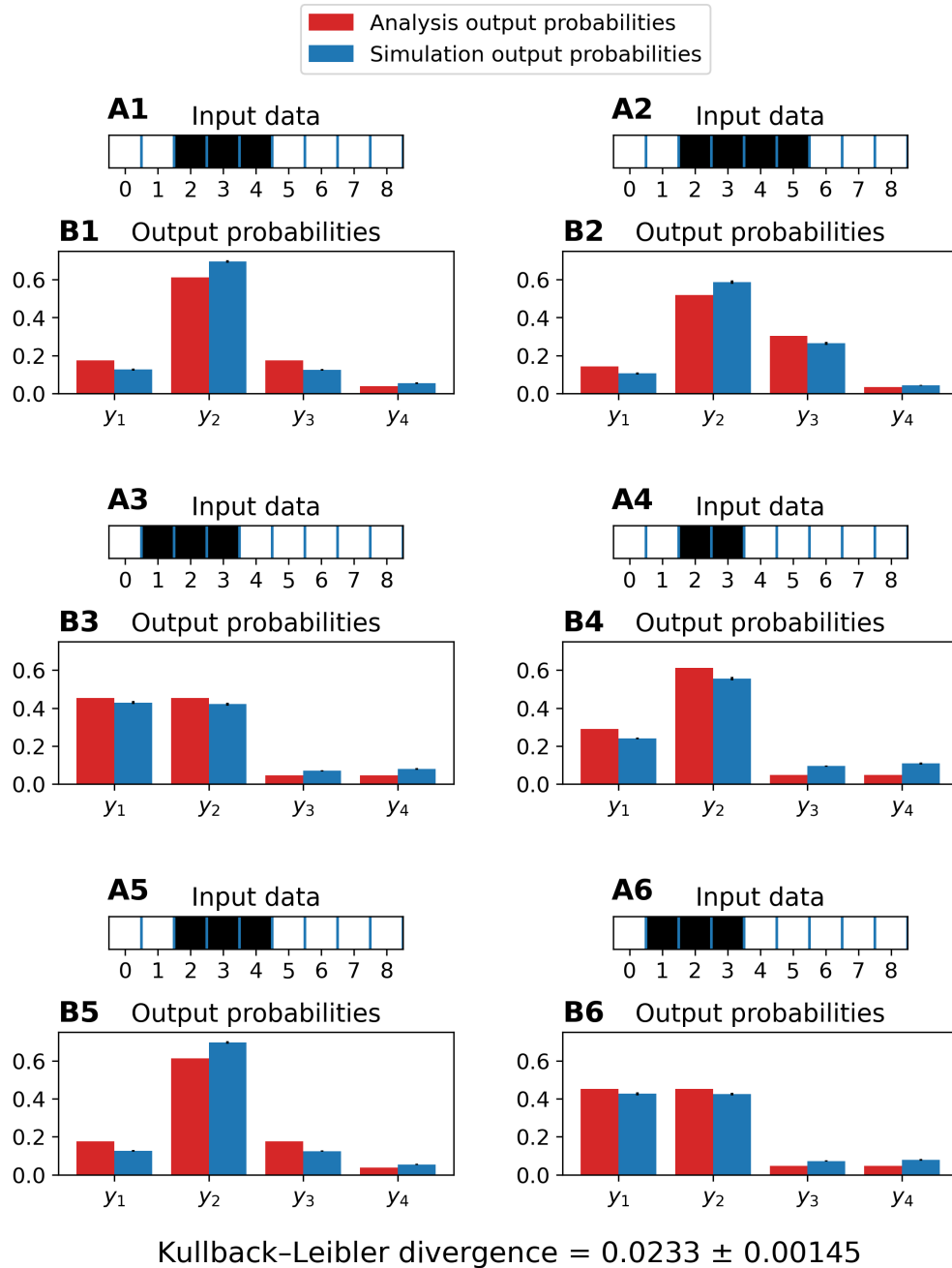


Figure 4.12: KL divergence for different  $f_{input}$  values. Hyperparameters:  $f_{prior} = 0\text{Hz}$ ,  $\tau_{decay} = 4\text{ms}$

	Image 1		Image 2	
	Analysis	Simulation	Analysis	Simulation
$y_0$	0.175	$0.126 \pm 0.0050$	0.143	$0.106 \pm 0.0054$
$y_1$	0.612	$0.695 \pm 0.0066$	0.518	$0.587 \pm 0.0098$
$y_2$	0.175	$0.124 \pm 0.0049$	0.304	$0.264 \pm 0.0072$
$y_3$	0.038	$0.054 \pm 0.0039$	0.035	$0.043 \pm 0.0028$
	Image 3		Image 4	
$y_0$	0.453	$0.429 \pm 0.0080$	0.291	$0.240 \pm 0.0044$
$y_1$	0.453	$0.421 \pm 0.0083$	0.613	$0.556 \pm 0.0084$
$y_2$	0.047	$0.070 \pm 0.0037$	0.048	$0.095 \pm 0.0036$
$y_3$	0.047	$0.080 \pm 0.0044$	0.048	$0.109 \pm 0.0058$
	Image 5		Image 6	
$y_0$	0.175	$0.125 \pm 0.0044$	0.453	$0.426 \pm 0.0085$
$y_1$	0.612	$0.697 \pm 0.0072$	0.453	$0.424 \pm 0.0068$
$y_2$	0.175	$0.124 \pm 0.0038$	0.047	$0.072 \pm 0.0031$
$y_3$	0.038	$0.054 \pm 0.0032$	0.047	$0.078 \pm 0.0047$

Table 4.3: Analysis and simulation output probabilities. Hyperparameters:  $f_{input} = 88\text{Hz}$ ,  $f_{prior} = 0\text{Hz}$ ,  $\tau_{decay} = 4\text{ms}$

## 4.2 Experiment 2: Mathematical analysis and simulation of the network with 1-D images



**Figure 4.13: Analysis and simulation result.** Hyperparameters:  $f_{input} = 88Hz$ ,  $f_{prior} = 0Hz$ ,  $\tau_{decay} = 4ms$  **A** Input images with  $9 \times 1$  pixels, active pixels in black. **B** Analytically calculated posterior probabilities and simulated posterior probabilities. The standard deviations are given by the black bars.

## 4 Experiments

---

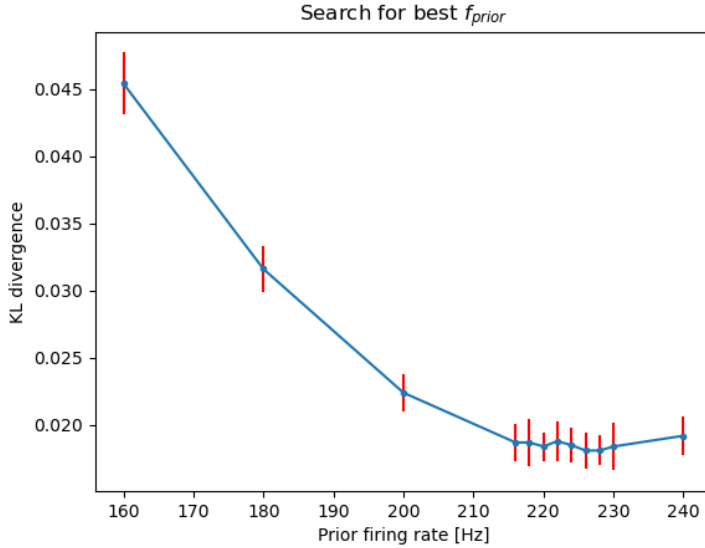


Figure 4.14: KL divergence for different  $f_{prior}$  values. Hyperparameters:  $f_{input} = 42\text{Hz}$ ,  $\tau_{decay} = 15\text{ms}$

and the best  $f_{prior}$  was searched.

$\tau_{decay} = 0.015\text{seconds}$ ,  $f_{input} = 42\text{Hz}$  The search for the best value of  $f_{prior}$  was performed in the same manner as for  $f_{input}$ . Values between 140 and 240 Hz were simulated and a prior firing rate of 222 Hz performed the best. The result of this search can be seen in Figure 4.14. The simulation results can be seen in Figure 4.15 and Table 4.4. In Figure 4.15 the value of the prior is indicated by the red border, which is three pixels wide and centered at the center position of the corresponding output class.

$\tau_{decay} = 0.004\text{seconds}$ ,  $f_{input} = 88\text{Hz}$  The search for the best value of  $f_{prior}$  was performed in the same manner as for  $f_{input}$ . Values between 360 and 460 Hz were simulated and a prior firing rate of 440 Hz performed the best. The result of this search can be seen in Figure 4.16. The results of this hyperparameter combination are given in Figure 4.17 and Table 4.5.

## 4.2 Experiment 2: Mathematical analysis and simulation of the network with 1-D images

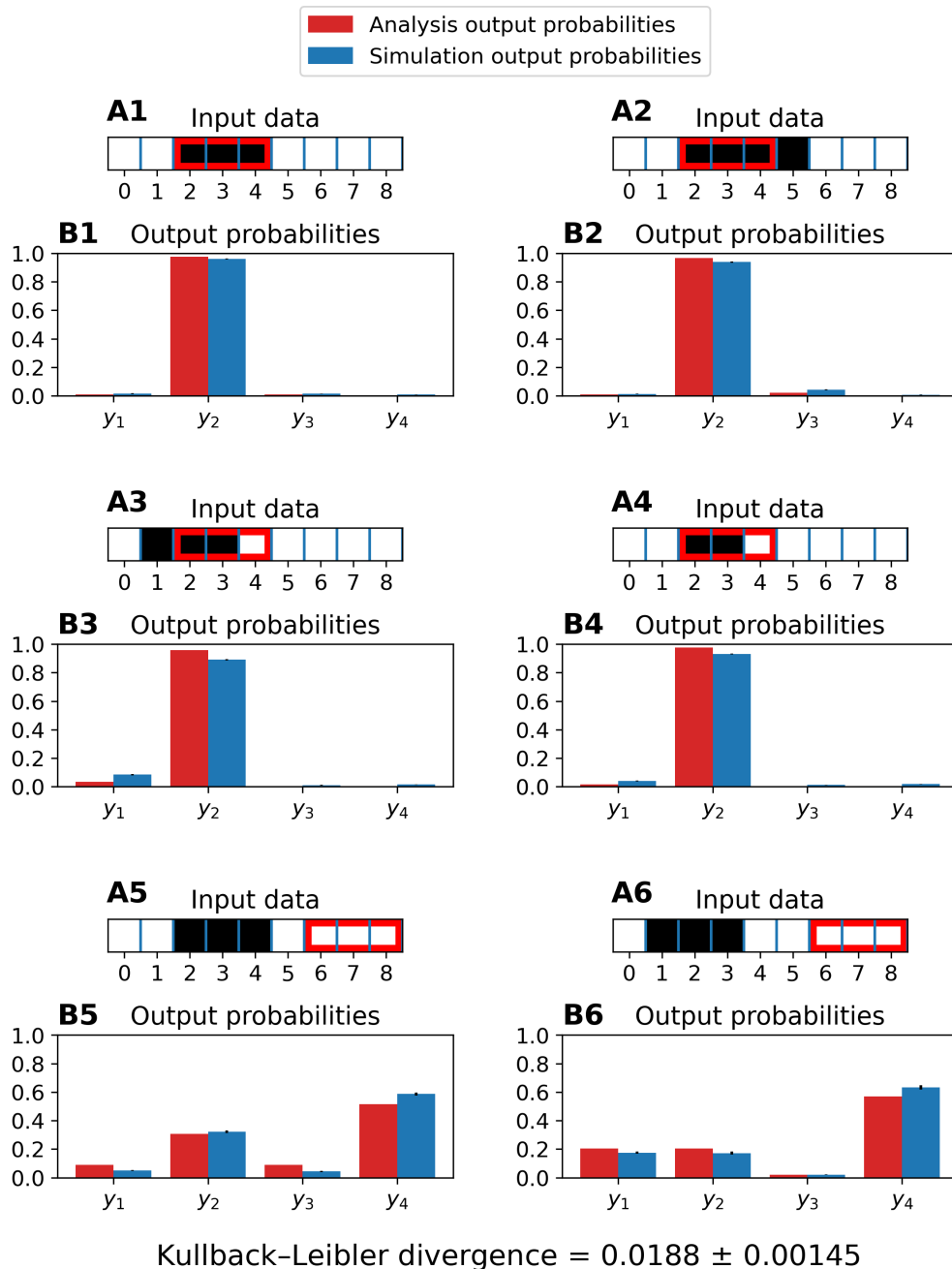


Figure 4.15: **Analysis and simulation result, active pixels in black.** Hyperparameters:  $f_{input} = 42Hz$ ,  $f_{prior} = 222Hz$ ,  $\tau_{decay} = 15ms$ . **A** Input images with  $9 \times 1$  pixels. Prior given as red border. **B** Analytically calculated posterior probabilities and simulated posterior probabilities. The standard deviations are given by the black bars.

## 4 Experiments

---

	Image 1		Image 2	
	Analysis	Simulation	Analysis	Simulation
$y_0$	0.010	$0.015 \pm 0.0021$	0.010	$0.013 \pm 0.0016$
$y_1$	0.977	$0.962 \pm 0.0030$	0.967	$0.938 \pm 0.0040$
$y_2$	0.010	$0.015 \pm 0.0017$	0.021	$0.042 \pm 0.0032$
$y_3$	0.002	$0.008 \pm 0.0016$	0.002	$0.007 \pm 0.0013$
	Image 3		Image 4	
$y_0$	0.035	$0.084 \pm 0.0038$	0.017	$0.039 \pm 0.0033$
$y_1$	0.957	$0.891 \pm 0.0046$	0.977	$0.931 \pm 0.0045$
$y_2$	0.004	$0.010 \pm 0.0018$	0.003	$0.012 \pm 0.0017$
$y_3$	0.004	$0.015 \pm 0.0016$	0.003	$0.018 \pm 0.0024$
	Image 5		Image 6	
$y_0$	0.088	$0.050 \pm 0.0033$	0.205	$0.175 \pm 0.0077$
$y_1$	0.308	$0.321 \pm 0.0087$	0.205	$0.172 \pm 0.0106$
$y_2$	0.088	$0.043 \pm 0.0039$	0.021	$0.021 \pm 0.0018$
$y_3$	0.515	$0.587 \pm 0.0105$	0.570	$0.632 \pm 0.0158$

Table 4.4: **Analysis and simulation output probabilities.** Hyperparameters:  $f_{input} = 42\text{Hz}$ ,  $f_{prior} = 222\text{Hz}$ ,  $\tau_{decay} = 15\text{ms}$

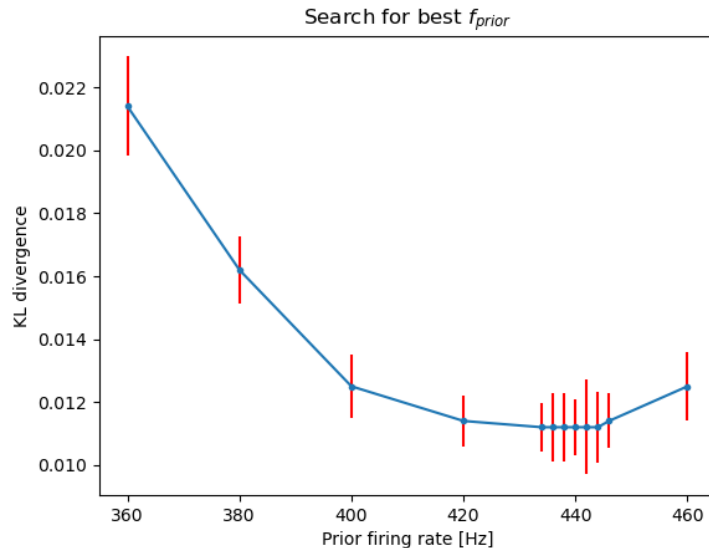


Figure 4.16: **KL divergence for different  $f_{prior}$  values.** Hyperparameters:  $f_{input} = 88\text{Hz}$ ,  $\tau_{decay} = 4\text{ms}$

## 4.2 Experiment 2: Mathematical analysis and simulation of the network with 1-D images

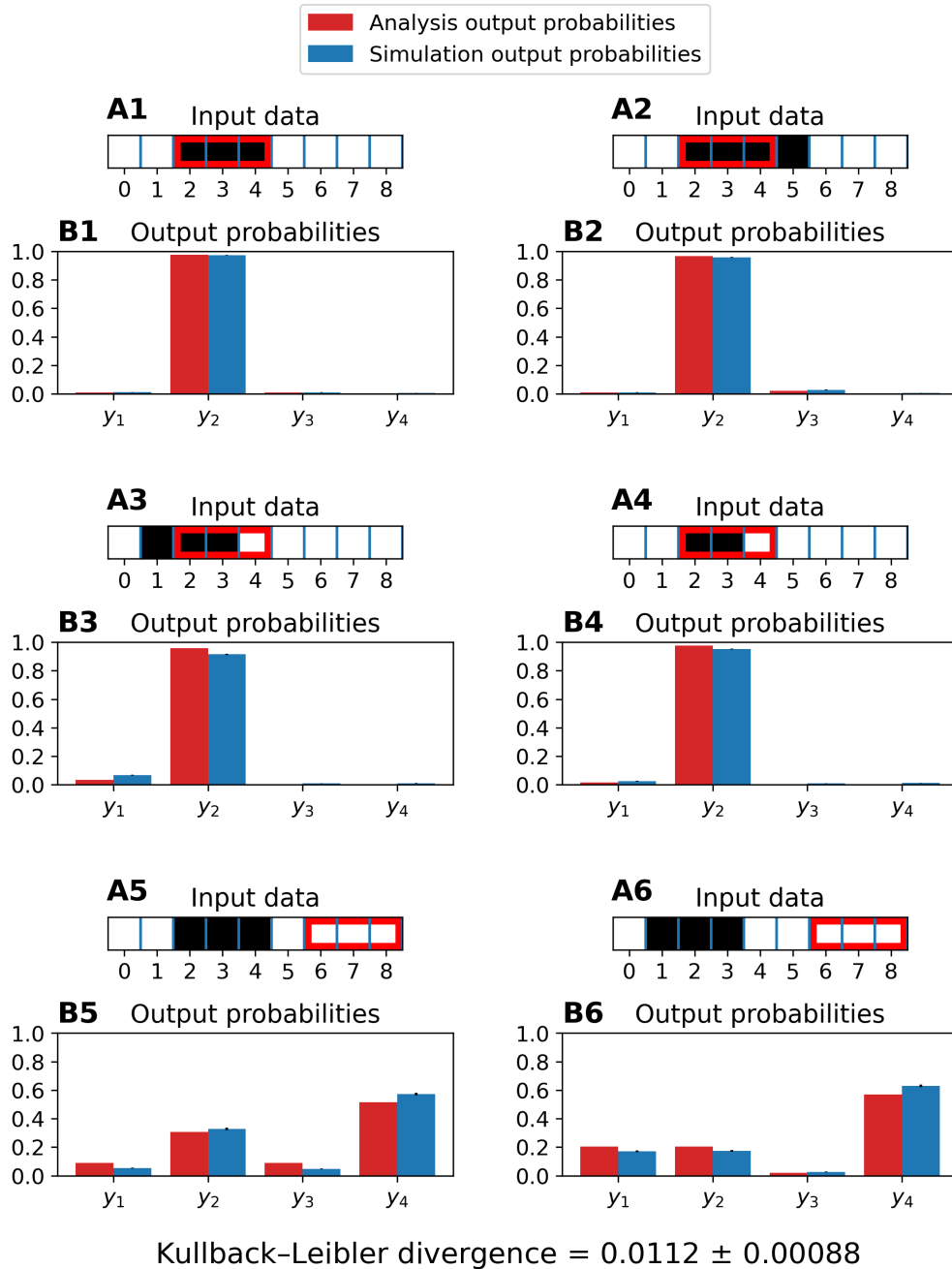


Figure 4.17: **Analysis and simulation result.** Hyperparameters:  $f_{input} = 88Hz$ ,  $f_{prior} = 440Hz$ ,  $\tau_{decay} = 4ms$  **A** Input images with  $9 \times 1$  pixels, active pixels in black. Prior given as red border. **B** Analytically calculated posterior probabilities and simulated posterior probabilities. The standard deviations are given by the black bars.

## 4 Experiments

---

	Image 1		Image 2	
	Analysis	Simulation	Analysis	Simulation
$y_0$	0.010	$0.011 \pm 0.0016$	0.010	$0.010 \pm 0.0017$
$y_1$	0.977	$0.974 \pm 0.0026$	0.967	$0.957 \pm 0.0034$
$y_2$	0.010	$0.010 \pm 0.0019$	0.021	$0.028 \pm 0.0036$
$y_3$	0.002	$0.005 \pm 0.0013$	0.002	$0.005 \pm 0.0011$
	Image 3		Image 4	
$y_0$	0.035	$0.066 \pm 0.0031$	0.017	$0.026 \pm 0.0030$
$y_1$	0.957	$0.915 \pm 0.0044$	0.977	$0.952 \pm 0.0039$
$y_2$	0.004	$0.009 \pm 0.0014$	0.003	$0.009 \pm 0.0017$
$y_3$	0.004	$0.011 \pm 0.0018$	0.003	$0.012 \pm 0.0020$
	Image 5		Image 6	
$y_0$	0.088	$0.052 \pm 0.0027$	0.205	$0.172 \pm 0.0061$
$y_1$	0.308	$0.328 \pm 0.0085$	0.205	$0.174 \pm 0.0059$
$y_2$	0.088	$0.046 \pm 0.0031$	0.021	$0.025 \pm 0.0025$
$y_3$	0.515	$0.573 \pm 0.0089$	0.570	$0.630 \pm 0.0095$

Table 4.5: **Analysis and simulation output probabilities.** Hyperparameters:  $f_{input} = 88\text{Hz}$ ,  $f_{prior} = 440\text{Hz}$ ,  $\tau_{decay} = 4\text{ms}$

To demonstrate the impact of rising  $f_{prior}$ , it was set to 600 Hz and the results can be seen in Figure 4.18 and Table 4.6.

$\tau_{decay} = 0.004\text{seconds}$ ,  $f_{input} = 98$ ,  $f_{prior} = 440\text{Hz}$  Finally, it was tested if an increase of  $f_{input}$  might decrease the Kullback-Leibler divergence even further. The network was simulated with increasing values of  $f_{input}$ , in steps of 2 Hz, beginning from 90 Hz. The result of this search can be seen in Figure 4.19. The best result was obtained with an input firing rate of 98 Hz. The results of that simulation can be seen in Figure 4.20 and Table 4.7.

**Approximating the analytic solution** After first finding the optimal  $f_{input}$  for disabled prior activity and then finding the optimal  $f_{prior}$  with enabled prior activity for  $\tau_{decay}$  the simulation was not yet approximating the analytical solution perfectly. Because of that, it was tried to raise  $f_{input}$ , to further decrease the Kullback-Leibler divergence. The search for a better  $f_{input}$  was

## 4.2 Experiment 2: Mathematical analysis and simulation of the network with 1-D images

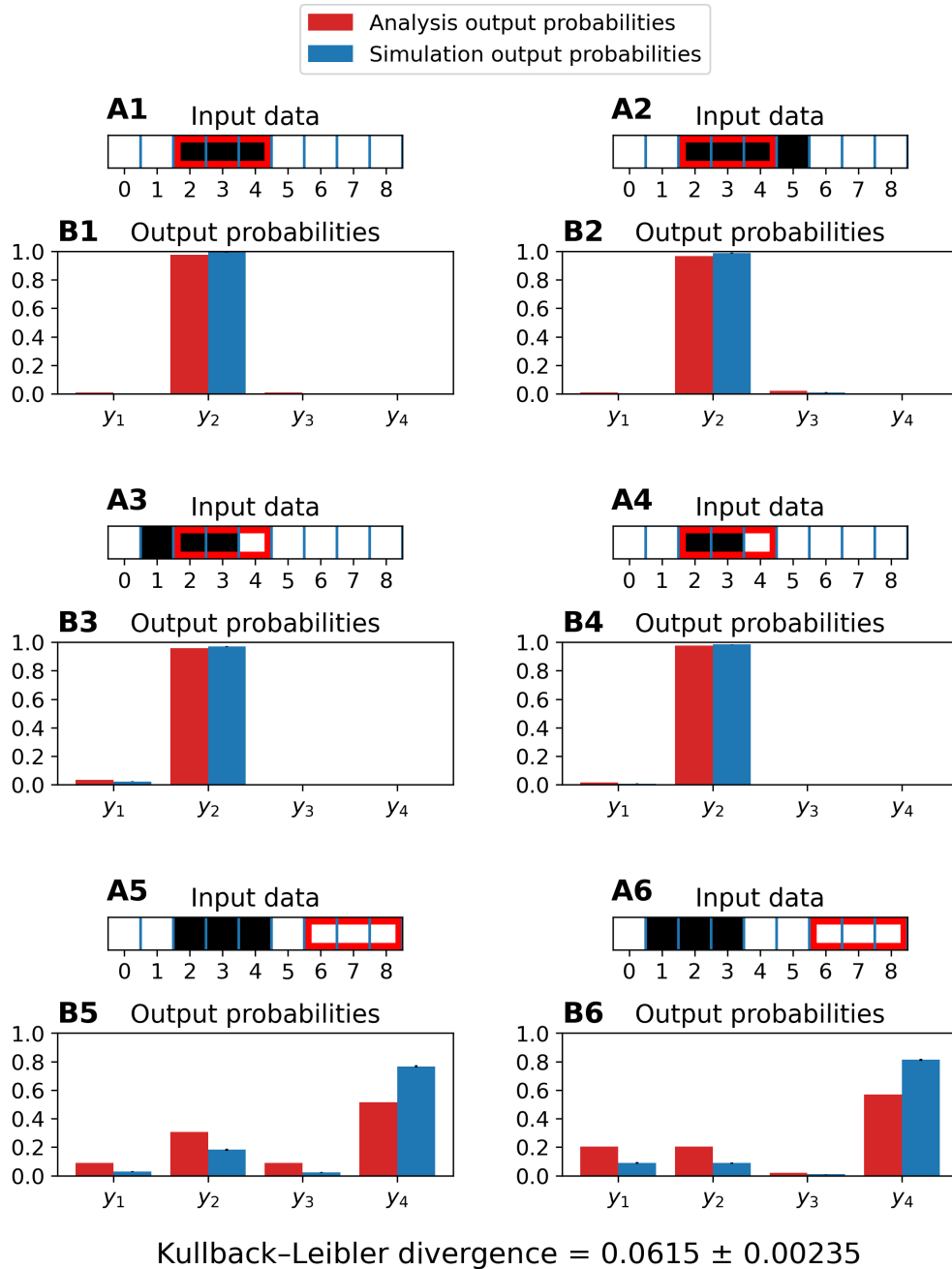


**Figure 4.18: Analysis and simulation result.** Hyperparameters:  $f_{input} = 88Hz$ ,  $f_{prior} = 600Hz$ ,  $\tau_{decay} = 4ms$ . **A** Input images with  $9 \times 1$  pixels, active pixels in black. Prior given as red border. **B** Analytically calculated posterior probabilities and simulated posterior probabilities. The standard deviations are given by the black bars.

## 4 Experiments

---

	Image 1		Image 2	
	Analysis	Simulation	Analysis	Simulation
$y_0$	0.010	$0.003 \pm 0.0011$	0.010	$0.003 \pm 0.0009$
$y_1$	0.977	$0.993 \pm 0.0013$	0.967	$0.987 \pm 0.0024$
$y_2$	0.010	$0.003 \pm 0.0008$	0.021	$0.009 \pm 0.0019$
$y_3$	0.002	$0.001 \pm 0.0005$	0.002	$0.001 \pm 0.0008$
	Image 3		Image 4	
$y_0$	0.035	$0.023 \pm 0.0025$	0.017	$0.008 \pm 0.0011$
$y_1$	0.957	$0.971 \pm 0.0030$	0.977	$0.984 \pm 0.0019$
$y_2$	0.004	$0.003 \pm 0.0009$	0.003	$0.003 \pm 0.0008$
$y_3$	0.004	$0.003 \pm 0.0011$	0.003	$0.004 \pm 0.0011$
	Image 5		Image 6	
$y_0$	0.088	$0.028 \pm 0.0026$	0.205	$0.089 \pm 0.0057$
$y_1$	0.308	$0.182 \pm 0.0077$	0.205	$0.088 \pm 0.0047$
$y_2$	0.088	$0.023 \pm 0.0025$	0.021	$0.010 \pm 0.0016$
$y_3$	0.515	$0.766 \pm 0.0079$	0.570	$0.813 \pm 0.0081$

Table 4.6: **Analysis and simulation output probabilities.** Hyperparameters:  $f_{input} = 88\text{Hz}$ ,  $f_{prior} = 600\text{Hz}$ ,  $\tau_{decay} = 4\text{ms}$

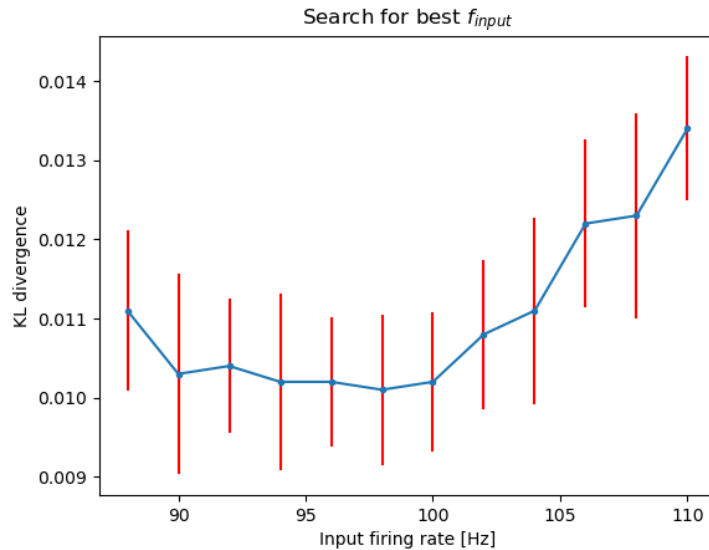


Figure 4.19: **KL divergence for different  $f_{input}$  values.** Hyperparameters:  $f_{prior} = 440\text{Hz}$ ,  $\tau_{decay} = 4\text{ms}$

## 4.2 Experiment 2: Mathematical analysis and simulation of the network with 1-D images

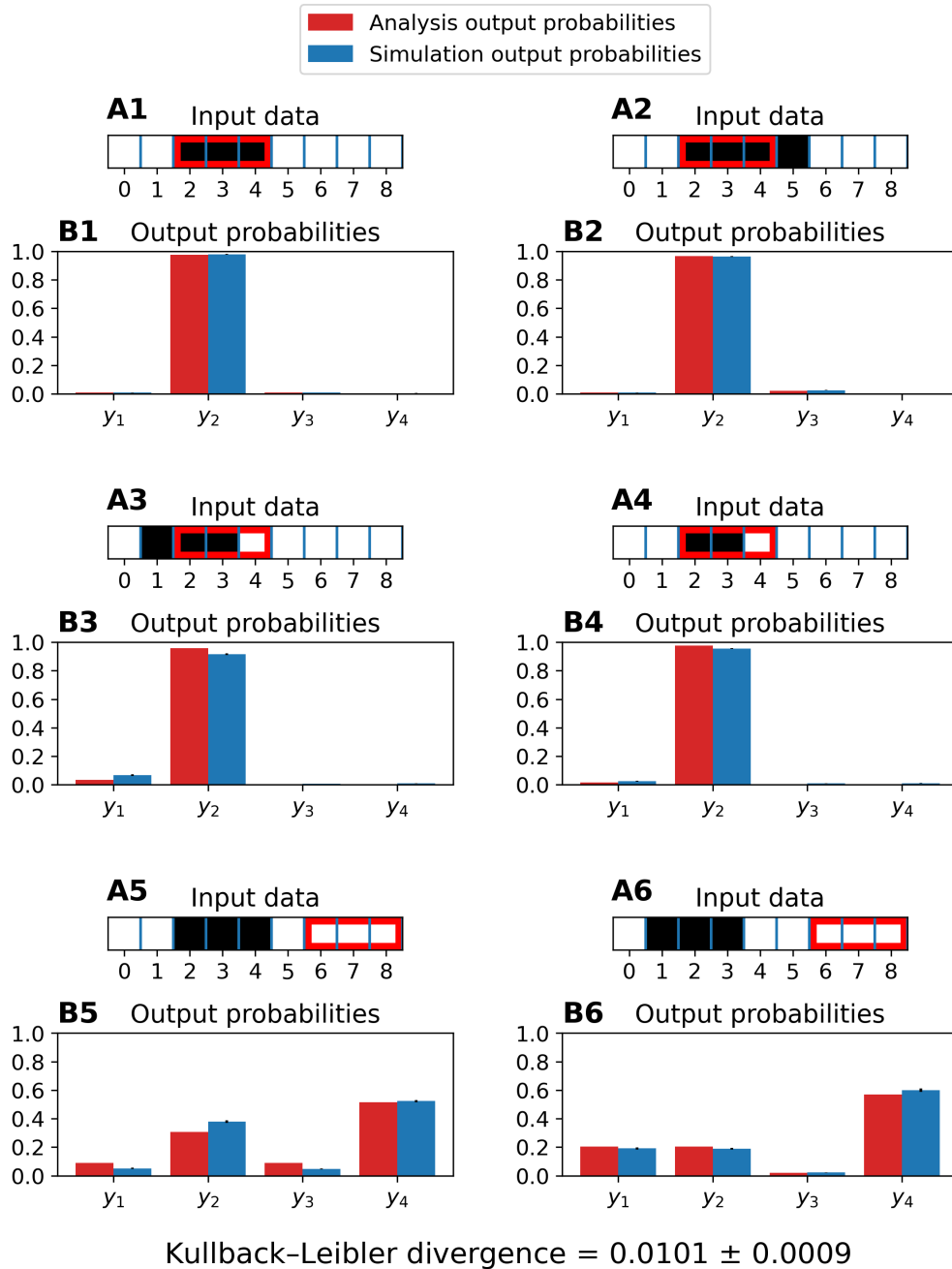


Figure 4.20: **Analysis and simulation result.** Hyperparameters:  $f_{input} = 98Hz$ ,  $f_{prior} = 440Hz$ ,  $\tau_{decay} = 4ms$  **A** Input images with  $9 \times 1$  pixels, active pixels in black. Prior given as red border. **B** Analytically calculated posterior probabilities and simulated posterior probabilities. The standard deviations are given by the black bars.

## 4 Experiments

---

	Image 1		Image 2	
	Analysis	Simulation	Analysis	Simulation
$y_0$	0.010	$0.009 \pm 0.0016$	0.010	$0.009 \pm 0.0015$
$y_1$	0.977	$0.979 \pm 0.0020$	0.967	$0.963 \pm 0.0023$
$y_2$	0.010	$0.009 \pm 0.0010$	0.021	$0.025 \pm 0.0020$
$y_3$	0.002	$0.004 \pm 0.0009$	0.002	$0.003 \pm 0.0008$
	Image 3		Image 4	
$y_0$	0.035	$0.067 \pm 0.0051$	0.017	$0.025 \pm 0.0031$
$y_1$	0.957	$0.916 \pm 0.0051$	0.977	$0.955 \pm 0.0033$
$y_2$	0.004	$0.007 \pm 0.0012$	0.003	$0.009 \pm 0.0012$
$y_3$	0.004	$0.009 \pm 0.0019$	0.003	$0.011 \pm 0.0019$
	Image 5		Image 6	
$y_0$	0.088	$0.051 \pm 0.0035$	0.205	$0.191 \pm 0.0080$
$y_1$	0.308	$0.379 \pm 0.0084$	0.205	$0.188 \pm 0.0061$
$y_2$	0.088	$0.046 \pm 0.0027$	0.021	$0.022 \pm 0.0021$
$y_3$	0.515	$0.523 \pm 0.0084$	0.570	$0.600 \pm 0.0116$

Table 4.7: **Analysis and simulation output probabilities.** Hyperparameters:  $f_{input} = 98\text{Hz}$ ,  $f_{prior} = 440\text{Hz}$ ,  $\tau_{decay} = 4\text{ms}$

performed for  $\tau_{decay} = 0.004\text{ms}$  and  $f_{prior} = 440\text{Hz}$ , as this set of hyperparameters performed the best overall. When comparing the former optimal result in Figure 4.17 with  $f_{input} = 88\text{Hz}$ , to the result with  $f_{input} = 98\text{Hz}$  in Figure 4.20, it can be seen that the Kullback-Leibler divergence decreased from 0.0112 to 0.0101. However, when comparing Tables 4.5 and 4.7, it can be seen that the higher  $f_{input}$  did not perform strictly better. The simulation output probabilities for Image 3 improved, while for Image 5 the output probability of  $y_2$  diverged more. A further increase of  $f_{input}$  started to increase the Kullback-Leibler divergence again, thus the final optimum of the hyperparameter set was reached. It was necessary to increase  $f_{input}$ , after  $f_{prior}$  was fitted, because the overall impact of  $f_{input}$  on the simulation decreased, due to the introduction of the prior activity.

## 4.3 Experiment 3: Transferability of hyperparameters

### 4.3.1 Introduction

In this experiment the optimal hyperparameters determined in Experiment 2 were used, while doubling the size of the network and input images of Experiment 2. The goal was to determine if the hyperparameters are universally applicable, regardless of the network size.

### 4.3.2 Methods

The number of input neurons was doubled from 18 to 36 neurons. This resulted in input images with 18 pixels. To double the effect of the prior neurons  $f_{prior}$  was doubled to 880 Hz, while the amount of the prior neurons was kept the same with 4 prior neurons. Furthermore, the matrix  $P^{X|Y}$  was doubled in size, by copying each value of the matrix to the right of itself. The rest of the methods were performed analogously to Experiment 2.

### 4.3.3 Results

The expanded matrix  $P^{X|Y}$  had its columns doubled, resulting in a dimension of  $[18 \times 4]$ . This yielded

$$P^{X|Y} = \begin{bmatrix} 0.9 & 0.9 & 0.9 & 0.9 & 0.9 & 0.9 & 0.1 & 0.1 & 0.1 & 0.1 & 0.1 & 0.1 & 0.1 & 0.1 & 0.1 & 0.1 & 0.1 & 0.1 \\ 0.1 & 0.1 & 0.1 & 0.1 & 0.9 & 0.9 & 0.9 & 0.9 & 0.9 & 0.9 & 0.9 & 0.9 & 0.9 & 0.9 & 0.9 & 0.9 & 0.9 & 0.9 \\ 0.1 & 0.1 & 0.1 & 0.1 & 0.1 & 0.1 & 0.1 & 0.1 & 0.9 & 0.9 & 0.9 & 0.9 & 0.9 & 0.9 & 0.9 & 0.9 & 0.9 & 0.9 \\ 0.1 & 0.1 & 0.1 & 0.1 & 0.1 & 0.1 & 0.1 & 0.1 & 0.1 & 0.1 & 0.1 & 0.1 & 0.9 & 0.9 & 0.9 & 0.9 & 0.9 & 0.9 \end{bmatrix}. \quad (4.13)$$

The simulation result for  $f_{input} = 98\text{Hz}$ ,  $f_{prior} = 880\text{Hz}$  and  $\tau_{decay} = 4\text{ms}$  can be seen in Figure 4.21 and Table 4.8. Initially, the Kullback-Leibler divergence

## 4 Experiments

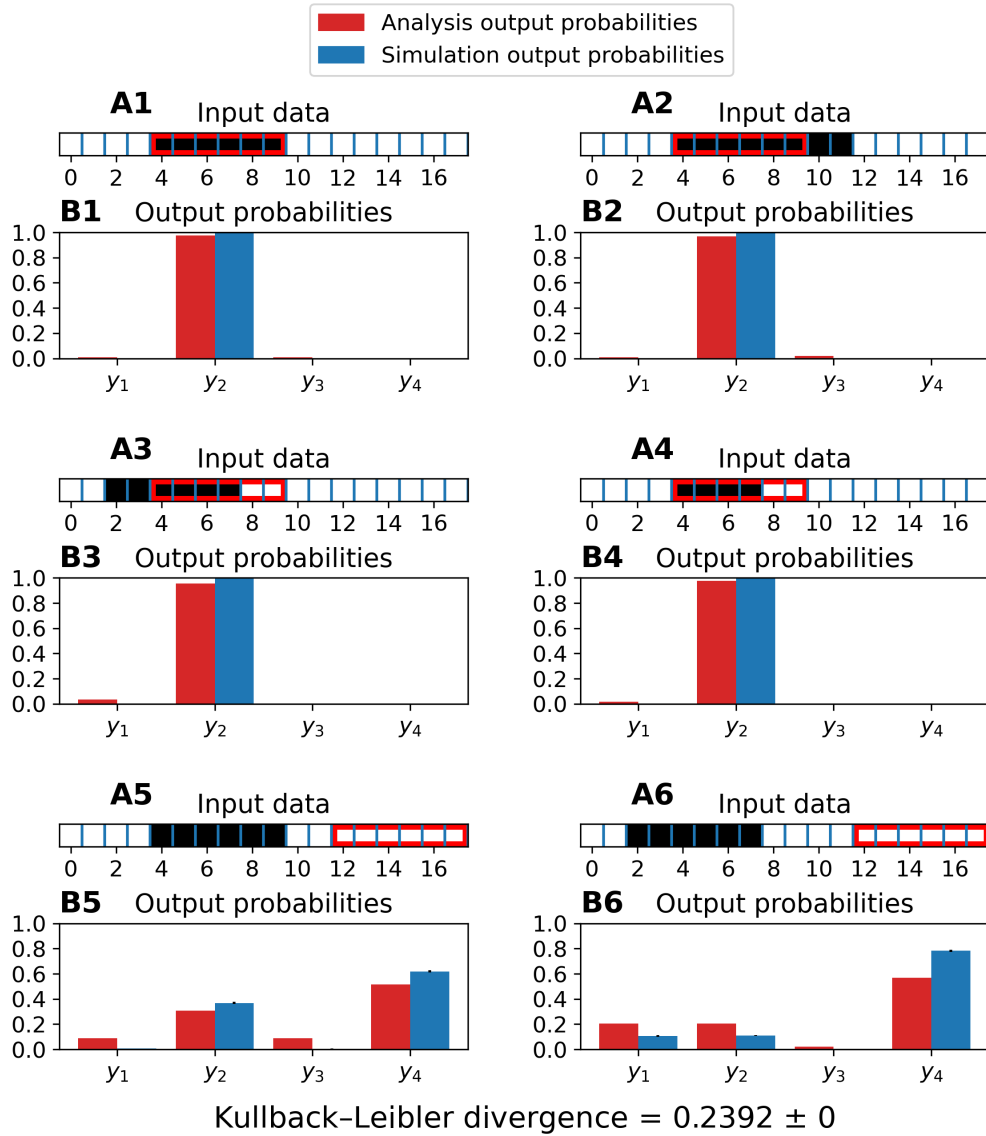
---

	Image 1		Image 2	
	Analysis	Simulation	Analysis	Simulation
$y_0$	0.010	$0.000 \pm 0.0001$	0.010	$0.000 \pm 0.0001$
$y_1$	0.977	$1.000 \pm 0.0002$	0.967	$1.000 \pm 0.0003$
$y_2$	0.010	$0.000 \pm 0.0001$	0.021	$0.000 \pm 0.0002$
$y_3$	0.002	$0.000 \pm 0.0000$	0.002	$0.000 \pm 0.0001$
	Image 3		Image 4	
$y_0$	0.035	$0.003 \pm 0.0010$	0.017	$0.000 \pm 0.0004$
$y_1$	0.957	$0.997 \pm 0.0010$	0.977	$1.000 \pm 0.0004$
$y_2$	0.004	$0.000 \pm 0.0001$	0.003	$0.000 \pm 0.0001$
$y_3$	0.004	$0.000 \pm 0.0001$	0.003	$0.000 \pm 0.0001$
	Image 5		Image 6	
$y_0$	0.088	$0.007 \pm 0.0010$	0.205	$0.106 \pm 0.0060$
$y_1$	0.308	$0.369 \pm 0.0096$	0.205	$0.109 \pm 0.0042$
$y_2$	0.088	$0.005 \pm 0.0010$	0.021	$0.001 \pm 0.0004$
$y_3$	0.515	$0.619 \pm 0.0098$	0.570	$0.783 \pm 0.0091$

Table 4.8: **Analysis and simulation output probabilities.** Hyperparameters:  $f_{input} = 98Hz$ ,  $f_{prior} = 880Hz$ ,  $\tau_{decay} = 4ms$

was infinite in this result, because some simulation output probabilities were zero and the Kullback-Leibler divergence is not defined for probabilities of zero. To circumvent this, an approximated Kullback-Leibler divergence was calculated, by setting the simulation output probabilities that were 0 to 0.0000001. This yielded a Kullback-Leibler divergence of 0.2392. This value was worse, compared to 0.0101 of the original network from Experiment 2. Thus, the hyperparameters were clearly not transferable to a network of double size.

### 4.3 Experiment 3: Transferability of hyperparameters



**Figure 4.21: Analysis and simulation result.** Hyperparameters:  $f_{input} = 98Hz$ ,  $f_{prior} = 880Hz$ ,  $\tau_{decay} = 4ms$  **A** Input images with  $18 \times 1$  pixels, active pixels in black. Prior given as red border. **B** Analytically calculated posterior probabilities and simulated posterior probabilities. The standard deviations are given by the black bars.

## 4.4 Experiment 4: Training of the network with 1-D images and predetermined hyperparameters

### 4.4.1 Introduction

In this Experiment the network of Experiment 2 was used, but the weights of the network were not derived from the matrices  $P^{X|Y}$  and  $P^{Y|Z}$ . Instead, they were learned from the input images. Through that, it could be analysed, how well the training process could approximate the analytical optimal weights and the posterior, when given the best hyperparameters. The goal of this experiment was to verify the training process, as well as to identify potential improvements to the training paradigm.

### 4.4.2 Methods

The network architecture was the same as in Experiment 2 and the training paradigm was the same as in Experiment 1. The used hyperparameters were  $f_{input} = 98\text{Hz}$ ,  $f_{prior} = 440\text{Hz}$  and  $\tau_{decay} = 4\text{ms}$ . The weight shifting hyperparameter  $c$  was determined via grid search.

### 4.4.3 Results

The Kullback-Leibler divergence for different values of  $c$  can be seen in Figure 4.22.

The training and evaluation results for the best value of  $c = 3$  can be seen in Figures 4.23, Figure 4.24 and Table 4.9.

The Kullback-Leibler divergence with  $c = 3$  was 0.0342. It was worse, compared to the best performing network of Experiment 2 with a Kullback-Leibler divergence of 0.0101. This means, that the training was imperfect and the network with the trained weights performed worse, than the one with calculated weights.

#### 4.4 Experiment 4: Training of the network with 1-D images and predetermined hyperparameters

---

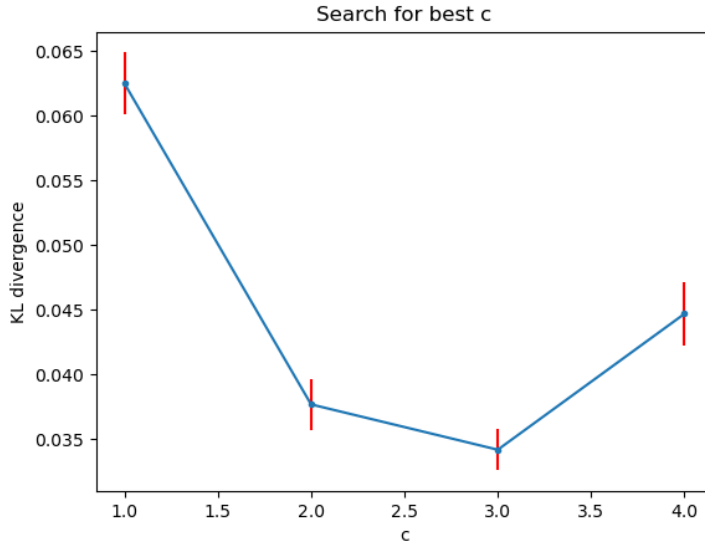
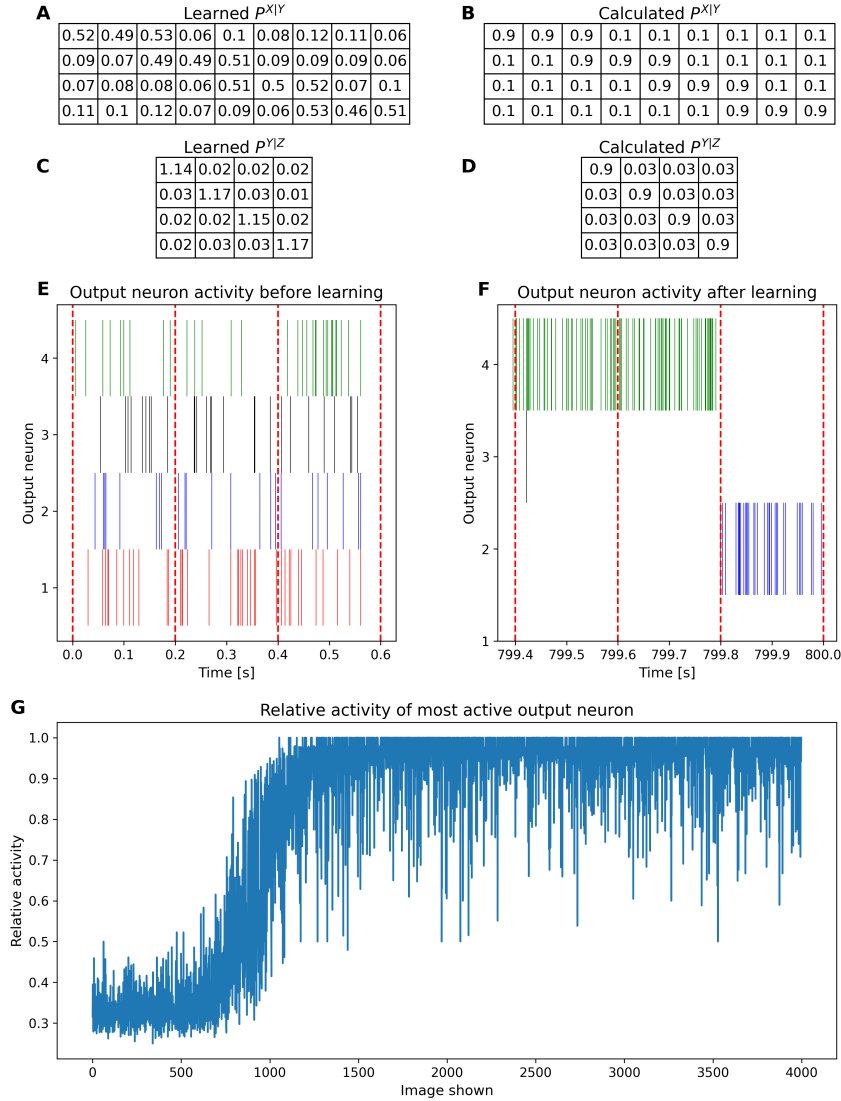


Figure 4.22: KL divergence for different c values  $f_{input} = 98\text{Hz}$ ,  $f_{prior} = 440\text{Hz}$ ,  $\tau_{decay} = 4\text{ms}$

	Image 1		Image 2	
	Analysis	Simulation	Analysis	Simulation
$y_0$	0.010	$0.004 \pm 0.0010$	0.010	$0.005 \pm 0.0009$
$y_1$	0.977	$0.988 \pm 0.0016$	0.967	$0.977 \pm 0.0028$
$y_2$	0.010	$0.005 \pm 0.0011$	0.021	$0.014 \pm 0.0018$
$y_3$	0.002	$0.003 \pm 0.0008$	0.002	$0.004 \pm 0.0012$
Image 3		Image 4		
$y_0$	0.035	$0.035 \pm 0.0026$	0.017	$0.012 \pm 0.0018$
$y_1$	0.957	$0.953 \pm 0.0035$	0.977	$0.977 \pm 0.0025$
$y_2$	0.004	$0.005 \pm 0.0010$	0.003	$0.004 \pm 0.0009$
$y_3$	0.004	$0.006 \pm 0.0014$	0.003	$0.006 \pm 0.0014$
Image 5		Image 6		
$y_0$	0.088	$0.039 \pm 0.0027$	0.205	$0.144 \pm 0.0053$
$y_1$	0.308	$0.202 \pm 0.0070$	0.205	$0.099 \pm 0.0049$
$y_2$	0.088	$0.032 \pm 0.0023$	0.021	$0.019 \pm 0.0021$
$y_3$	0.515	$0.727 \pm 0.0063$	0.570	$0.738 \pm 0.0074$

Table 4.9: Analysis and simulation output probabilities. Hyperparameters:  $f_{input} = 98\text{Hz}$ ,  $f_{prior} = 440\text{Hz}$ ,  $\tau_{decay} = 4\text{ms}$ ,  $c = 3$

## 4 Experiments



**Figure 4.23: Training result.** Hyperparameters:  $f_{input} = 98\text{Hz}$ ,  $f_{prior} = 440\text{Hz}$ ,  $\tau_{decay} = 4\text{ms}$ ,  $c = 3$  **A** The learned probability matrix  $P^{X|Y}$ . It was determined by taking the weights to the power of e. **B** The calculated probability matrix  $P^{X|Y}$ . **C** The learned prior probability matrix  $P^{Y|Z}$ . **D** The calculated prior probability matrix  $P^{Y|Z}$ . **E, F** Spike activity expressed by the output neurons before and after the training of the network. **G** This shows the number of spikes the most active output neuron generated, relative to the number of spikes all other output neurons generated combined.

#### 4.4 Experiment 4: Training of the network with 1-D images and predetermined hyperparameters

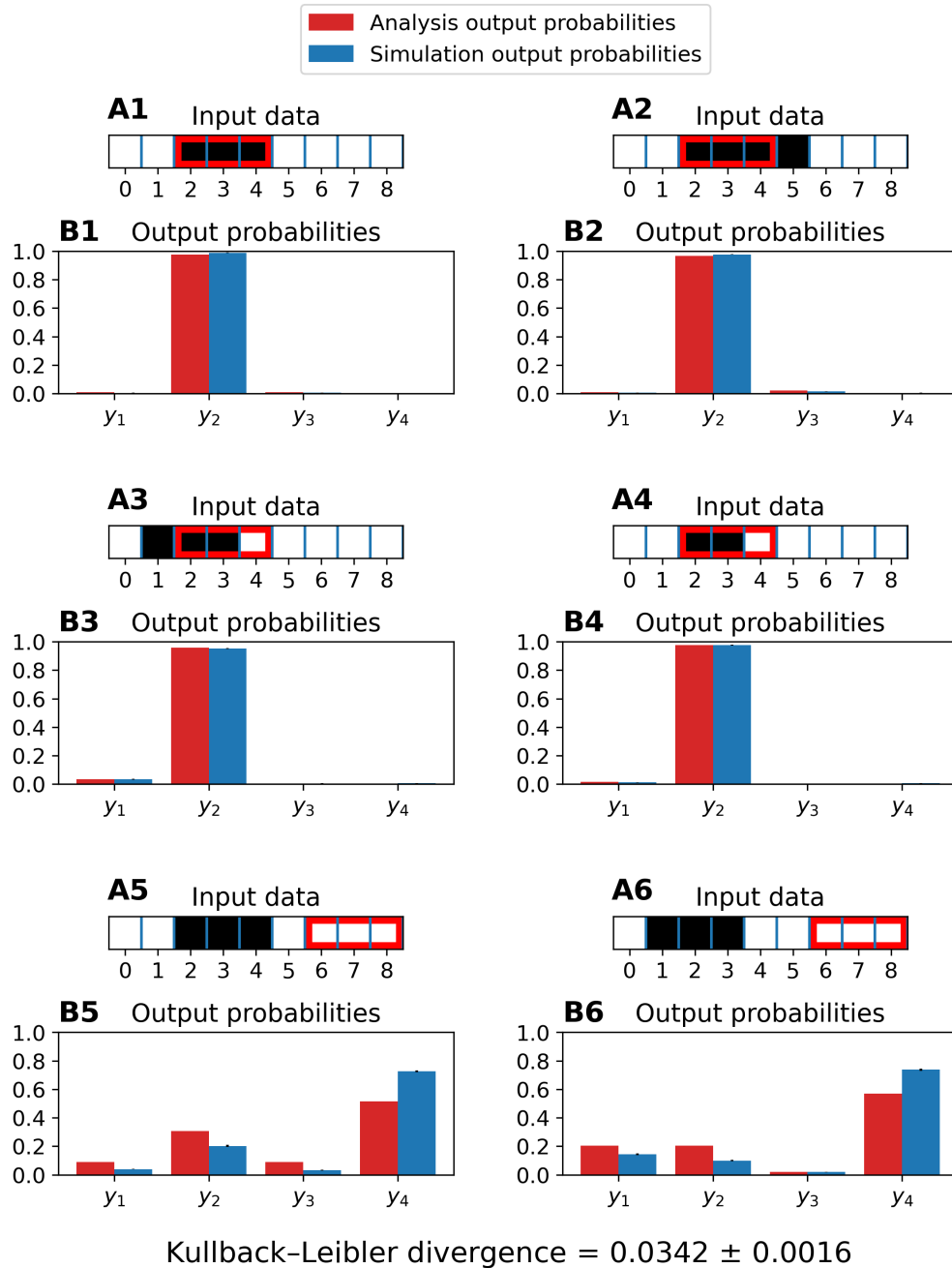


Figure 4.24: **Analysis and simulation result.** Hyperparameters:  $f_{input} = 98\text{Hz}$ ,  $f_{prior} = 440\text{Hz}$ ,  $\tau_{decay} = 4\text{ms}$ ,  $c = 3$  **A** Input images with  $9 \times 1$  pixels, active pixels in black. Prior given as red border. **B** Analytically calculated posterior probabilities and simulated posterior probabilities. The standard deviations are given by the black bars.



# 5 Discussion

## 5.1 Impact of the hyperparameters

To further the understanding of the network model, each hyperparameter was analysed within Experiment 2.

$f_{input}$   $f_{input}$  controls how strongly the information of the input image is weighed. This means that by raising  $f_{input}$  the impact of the active pixels increases, while the impact of the prior neuron decreases comparatively. This effect will be explained in the following paragraph about  $f_{prior}$ . Furthermore, by raising  $f_{input}$  the membrane potentials of all output neurons are raised equally by the same percentage. However, this causes difficulties when trying to determine the optimal  $f_{input}$ . When raising  $f_{input}$ , it was also observed, that the posteriors of output classes adjacent to the active pixels decreased. This can be observed when comparing Tables 4.1 and 4.2, where  $f_{input}$  was raised from 42 Hz to 70 Hz. For example, when looking at Image 4 in the mentioned tables, it can be seen that for  $f_{input} = 42\text{Hz}$  the simulation output probability of  $y_1$  is 0.245. This probability is due to the active pixel at position 2, which belongs to class 1 and 2 at the same time.  $y_2$  has a higher simulation output probability of 0.553, as it has two active pixels within its active area. When increasing  $f_{input}$  to 70 Hz one might expect the probabilities for  $y_1$  and  $y_2$  to rise. However, this does not happen, instead the simulation output probability for  $y_1$  fell to 0.207, while for  $y_2$  it rose to 0.685. It is assumed that this happened, because the membrane potentials of the output neurons were never normalized. As the input neurons spike more quickly, the membrane potential of  $y_1$  rose by a smaller amount than the membrane potential of  $y_2$ , as there was one more active pixel within the active area of  $y_2$ . As given by Equation 3.17  $q_k$

## 5 Discussion

---

depends exponentially on  $u_k$ . It is important to notice, that all  $q_k$  together yield the discrete probability density function of the posterior. When  $f_{input}$  is increased, all membrane potentials increase by the same percentage. Due to the exponential dependency of the probability density function on the membrane potentials, the different  $q_k$ , however, do not all change by the same percentage. Rather, every  $q_k$  increases by a different percentage, the  $q_k$  of  $y_k$  with the most active pixels by the smallest amount and the  $q_k$  of the  $y_k$  with the least active pixels by the smallest percentage. However, this behaviour might be desired, as generating more input spikes corresponds stochastically to generating more samples from the likelihood. Taking more samples reduces the standard error of the posterior probability distribution, thus reducing the width of its probability density function around  $q_k$ , whose  $y_k$  has the most active pixels. This means, that the more samples of the input the network takes, the more certain it becomes of the most likely option.

$f_{prior}$  When increasing the prior firing rate, the impact on the result of the prior neurons increased, while the impact of the input neurons decreased comparatively. This behaviour can be seen when comparing Figures 4.17 and 4.18. They show the results for  $f_{input} = 88\text{Hz}$ ,  $\tau_{decay} = 4\text{ms}$  and  $f_{prior} = 440$  and  $600\text{Hz}$  respectively. In Subfigure B6, the input image lay in the middle of the active areas of  $y_1$  and  $y_2$ , while the prior neuron  $z_4$  was active. When  $f_{prior}$  was increased, the simulation output probability of  $y_4$  rose, while all other probabilities fell. The opposite behaviour was observed when raising  $f_{input}$  instead. The same changing of the probability density function of the posterior, as observed for  $f_{input}$ , was expected, as the prior neurons contribute to  $u_k$  in the same way, as the input neurons. However, it was impossible to observe it separately, as increasing  $f_{prior}$  inherently has the same effect. Per design, the prior neurons had the effect of narrowing, or widening the probability density function of the posterior, around the  $q_k$ , which is supported by the prior. This made the two effects indistinguishable from each other.

$\tau_{decay}$   $\tau_{decay}$  determines for how long and how strongly an input or prior spike contributes to the membrane potentials of the output neurons. The bigger  $\tau_{decay}$  is, the smaller  $f_{input}$  and  $f_{prior}$  need to be, to minimize the

Kullback-Leibler divergence. This is represented by the final hyperparameters for  $\tau_{decay}$  of 4 and 15 ms. While for  $\tau_{decay} = 15\text{ms}$  the best input firing rate was 42 Hz and the prior firing rate was 222 Hz, for  $\tau_{decay} = 4\text{ms}$  they had to be raised to 98 and 440 Hz to minimize the Kullback-Leibler divergence.

## 5.2 Basis of the network model

In this thesis a hierarchical spiking Winner-Take-All neural network model, which was based on Nessler et al. (2013) and expanded by a neuron layer of prior neurons was used. The first hypothesis the network model is based on, is that  $q_k$  is equal to the posterior probability  $P(Y = k|X, Z)$ . This relation was explained in Section 3.4 and found conclusive. This model is also based on the hypothesis, that the weights of the network, due to STDP-induced changes, converge stochastically to the log of the conditional probability, that a presynaptic neuron has fired shortly before the postsynaptic neuron. This relation, given in Equation 3.20, was proven in Experiment 2. The likelihood  $P(X = x|Y = k)$ , the prior  $P(Y = k|Z = j)$  and the posterior  $P(Y = k|X, Z)$  were analytically calculated. Then the input weights were derived from the likelihood and the prior weights were derived from the prior. Next, the network was simulated and its output was used to calculate the posterior of the simulation. The Kullback-Leibler divergence between the analytically calculated posterior and the posterior of the simulation was calculated, to evaluate how closely the simulation was able to approximate the optimal analytical solution. The results of the best hyperparameter set are given in Figure 4.20 and Table 4.7. The simulation approximated the analytical solution closely and it can be concluded, that the hypothesis of Equation 3.20 was correct. However, it was not possible to tune the network to perfectly match the analytical solution. One difficulty when tuning the network was, that increasing or decreasing  $f_{input}$  had an unexpected effect of changing the probability density function of the posterior. This effect was explained in Section 5.1. However, it is unclear why the analytic posterior could not be approximated closer, as the impacts of  $f_{input}$ , as well as  $f_{prior}$  seemed correct. It might be possible, that varying the hyperparameter  $\sigma$  would improve the training result.

## 5.3 Reproducing behaviours of the visual cortex

The experiments yielded evidence, that a spiking Winner-Take-All neural network can recreate behaviours, that were observed in the visual cortex. Neural feedback is most commonly associated with attention. Such attention behaviour could be shown in Experiment 1, where ambiguous cross images were shown to the network. Without the feedback and with perfectly trained output neurons the network would not have known, which part of the cross image to focus on. In reality, the output neurons ended up with different sized active areas and unequal relative activities. Due to that, when both parts of the cross were exactly in the middle of the theoretical centers of two output neurons, one output neuron was more active than the other. The network put its attention on either the horizontal or vertical part of the cross, even with inactive prior neurons. However, this unequal learning of the output neurons was no disturbance, as the feedback of the prior neurons could offset those errors. If the prior activity was set to "horizontal", the corresponding output neuron was always more active, than its vertical counterpart, even if the vertical neuron had a higher relative activity without the prior. The impact of the prior neurons was interpreted as the network putting attention on the corresponding part of the cross.

As shown by Lee TS (2003), feedback from the inferior temporal cortex to V1 is able to convince V1 into "seeing" illusory lines. This behaviour was reproduced in Experiment 2. Figures 4.13 and 4.17 show the validation results of the same network with the same hyperparameter set, except once with disabled prior neurons and once with enabled ones. The sixth input image has active pixels at positions 1, 2 and 3. Thus, it lies in the middle between classes 1 and 2. When looking at Figure 4.13A6 and B6 it can be seen that with disabled prior neurons most of the output activity originates from  $y_1$  and  $y_2$ , the output of the network matches the visual input. In Figure 4.17 with a prior that signals class 4 in Subfigures A6 and B6 it can be seen that the output probabilities shifted. The most active output neuron now is  $y_4$ , while  $y_1$  and  $y_2$  have smaller output probabilities.  $y_4$ , being the most active neuron, contradicts the visual input, but it is enforced by the prior information it receives. This feedback induced belief matched the experimental evidence of the visual cortex.

## 5.4 Reusing hyperparameters for networks of different size

The possibility to reuse a hyperparameter set for a network of different size was examined in Experiment 3. In this experiment the number of input neurons, the prior firing frequency and the size of the input images was doubled, compared to Experiment 2. Then the weights were re-calculated, according to the bigger size. When comparing Figures 4.20 and 4.21 it can be seen, that the analysis output probabilities stayed the same. This was expected, as by doubling the pixels of the input images the information within them did not change. The areas corresponding to an output class doubled in size, as did the active pixels shown in black. The Kullback-Leibler divergence of this experiment was 0.2392 compared to 0.0101 of the original network. Furthermore, in Experiment 1 the best value of  $c$  was determined as 20, while in Experiment 4 it was 3. This indicates, that the best value of  $c$  is dependent on the network's size,  $f_{input}$ ,  $f_{prior}$  and  $\tau_{decay}$ . It was suspected that  $c$  converges towards a value, which ensures that the potentiation term of  $\Delta w$  is in the right proportion to the depression term. This clearly showed, that the hyperparameters could not simply be reused for a network of different size. One possible reason for this could be the, discussed in Section 5.1, effect of different  $f_{input}$  changing the probability density function of  $q_k$ . By doubling the number of input neurons, twice as many samples were pulled from the input probability distribution, which made the network prefer output classes with more active pixels within their active areas over output classes with fewer active pixels. Furthermore, the impact of the prior neurons was too high, as seen in Figure 4.21B6. As discussed in Section 5.1, the exponential dependency of  $q_k$  on  $u_k$  might have caused this increased impact of the prior neurons. For each validation image only one of the four output neurons received EPSPs from the active prior neuron, when noise is disregarded. By raising its  $u_k$  to the power of e, its proportion to the other membrane potentials got bigger, than before the doubling of  $f_{prior}$ . This increased impact of the prior neurons is suspected to be the main reason why the transfer of the hyperparameters performed poorly.

## 5.5 Training weights with predetermined hyperparameters

In Experiment 4 the best hyperparameter set of Experiment 2 was used to train the input and prior weights of the network. The goal of this was to determine how well the network could approximate the optimal weights and the posterior. Only the weight shifting hyperparameter  $c$  was varied, to minimize the Kullback-Leibler divergence. With the best value of  $c = 3$  the Kullback-Leibler divergence was 0.0342 compared to 0.0101 of the network with the calculated weights from Experiment 2. When comparing the likelihood and prior probability matrices in Figure 4.23 it can be seen that the network learned the correct discrimination function. However, the likelihood values were too small, while the prior values were too big. This observation explains why further raising the value of  $c$  did not lower the Kullback-Leibler divergence, as the weights of the network are proportional to the mentioned probabilities. As raising  $c$  increases both likelihood and prior probabilities, it is impossible to further increase the likelihood probabilities, while also decreasing the prior probabilities. By adding a second separate weight shifting hyperparameter, it would be possible to increase the values of the input weights and to decrease the values of the prior weights at the same time. This would improve the performance of the trained network and might also grant more precise control over the output of the network.

## 5.6 Future work

The narrowing and widening of the probability density function of the posterior, when changing  $f_{input}$ , caused problems in this thesis and the model could potentially be improved by analysing it further. It was caused by the exponential dependency of  $q_k$  on  $u_k$ , which seems intended and indicates that this behaviour was not caused by an implementation error of the model. It would be interesting to remove the exponential dependency to determine if the changing of the probability density function of the posterior disappears. Furthermore, it could be tested if the hyperparameters

of the network would be reusable for networks of different sizes when the exponential dependency is removed.

The network architecture could be expanded by adding additional layers or networks, to increase the complexity of the experiment paradigms. For now, the prior neurons were told what feedback to give, but they could also receive input from another network. For example, a network modelling the inferior temporal cortex could deliver the prior, just as observed in biology. Another idea would be to add a network, which models a different sensory part of the brain. One could utilize audio signals, to train a second network, which then provides context about different environments the visual input might be coming from. For example, when looking at an ambiguous image, that might represent a human face, hearing human language might enforce that belief. When hearing bird chatter and the rustling of leaves, however, it might change the belief into seeing just parts of a tree, that look similar to a face. In the brain, the inferior temporal cortex receives feedback on how its own feedback impacted V1 via the visual pathway. This part of the feedback loop was neglected in the network architecture. The prior neurons could be fed the output of this thesis' network. Through that, the feedback loop would be complete.

Experiment 4 showed problems, that were caused by having only a single weight shifting hyperparameter for both input and prior weights. A second separate weight shifting parameter could be implemented, to quickly resolve this problem. A more sophisticated solution could be to design a variable weight shifting parameter, that depends on characteristics of the network and its neurons. The experiments suggested, that  $c$  depends on the network's size,  $f_{input}$ ,  $f_{prior}$  and  $\tau_{decay}$ . Thus, a variable weight shifting parameter could be designed, which depends on these hyperparameters.

Pfister and Gerstner (2006) reported, that pair-based STDP was not sufficient to explain synaptic changes, triggered by triplet or quadruplet spikes, observed in neurons. They showed that a triplet learning rule was able to approximate experimental data better. As the training in Experiment 4 prove imperfect, it could probably be improved, by using a more complex learning rule.

This thesis provided insight about the hierarchical spiking Winner-Take-All network model. The network from Nessler et al. (2013) was successfully

## 5 Discussion

---

used as a template and was expanded by a layer, representing a-priori information. It was demonstrated, that the model was able to reproduce behaviours like attention and changing of belief through feedback. Through the insights of the experiments, several ideas of how to analyse and improve the model further were found.

# Bibliography

- Arbib, Michael A. (2003). *The handbook of brain theory and neural networks 2nd Edition*. Cambridge, MA, USA: MIT Press, pp. 1228–1231. ISBN: 0-262-01197-2 (cit. on p. 5).
- Contreras, Diego (2004). “Electrophysiological classes of neocortical neurons.” In: *Neural Networks 17.5. Vision and Brain*, pp. 633–646. ISSN: 0893-6080. DOI: <https://doi.org/10.1016/j.neunet.2004.04.003>. URL: <https://www.sciencedirect.com/science/article/pii/S0893608004000863> (cit. on p. 5).
- Dan Yang, Poo Mu-Ming (2004). “Spike timing-dependent plasticity of neural circuits.” In: *Neuron 44*, pp. 23–30. DOI: [10.1016/j.neuron.2004.09.007](https://doi.org/10.1016/j.neuron.2004.09.007) (cit. on p. 2).
- Darlington, Timothy R, Jeffrey M Beck, and Stephen G Lisberger (Oct. 2018). “Neural implementation of Bayesian inference in a sensorimotor behavior.” en. In: *Nat. Neurosci. 21.10*, pp. 1442–1451 (cit. on p. 8).
- Feldman, Daniel E. (2012). “The Spike-Timing Dependence of Plasticity.” In: *Neuron 75.4*, pp. 556–571. ISSN: 0896-6273. DOI: <https://doi.org/10.1016/j.neuron.2012.08.001>. URL: <https://www.sciencedirect.com/science/article/pii/S0896627312007039> (cit. on p. 2).
- Funamizu Akihiro Kuhn Bernd, Doya Kenji (Dec. 2016). “Neural substrate of dynamic Bayesian inference in the cerebral cortex.” In: *Nature Neuroscience 19*. DOI: [doi:10.1038/nrn.4390](https://doi.org/10.1038/nrn.4390) (cit. on pp. 1, 8).
- Gerstner, Wulfram and Werner M. Kistler (2002). *Spiking Neuron Models: Single Neurons, Populations, Plasticity*. Cambridge University Press (cit. on pp. 1, 8, 10, 11).
- Guo, Shangqi et al. (2019). “Hierarchical Bayesian Inference and Learning in Spiking Neural Networks.” In: *IEEE Transactions on Cybernetics 49.1*, pp. 133–145. DOI: [10.1109/TCYB.2017.2768554](https://doi.org/10.1109/TCYB.2017.2768554) (cit. on p. 2).
- Huff T Mahabadi N, Tadi P. (2024). *StatPearls [Internet]*. StatPearls Publishing. Chap. Neuroanatomy, Visual Cortex. (Cit. on p. 7).

## Bibliography

---

- Jolivet, Renaud et al. (Aug. 2006). "Predicting spike timing of neocortical pyramidal neurons by simple threshold models." In: *Journal of Computational Neuroscience* 21.1, pp. 35–49. ISSN: 1573-6873. doi: [10.1007/s10827-006-7074-5](https://doi.org/10.1007/s10827-006-7074-5) (cit. on p. 19).
- Jones EG; Hendry, SHC, ed. (1984). *Cerebral cortex: cellular components of the cerebral cortex*. New York: Plenum Press. Chap. Basket cells, pp. 309–334 (cit. on p. 5).
- Joyce, James (2019). "Bayes' Theorem." In: *The Stanford Encyclopedia of Philosophy*. Ed. by Edward N. Zalta. Spring 2019. Metaphysics Research Lab, Stanford University (cit. on p. 13).
- Korb, K B and A E Nicholson (2011). "Inference in Bayesian Networks." In: *Bayesian Artificial Intelligence*. CRC Press, pp. 55–95 (cit. on p. 14).
- Lee TS, Mumford D. (July 2003). "Hierarchical Bayesian inference in the visual cortex." In: *J Opt Soc Am A Opt Image Sci Vis.* doi: [10.1364/josaa.20.001434](https://doi.org/10.1364/josaa.20.001434) (cit. on pp. vii, 1, 3, 6, 8, 9, 68).
- Maass, Wolfgang (Nov. 2000). "On the Computational Power of Winner-Take-All." In: *Neural Computation* 12.11, pp. 2519–2535. ISSN: 0899-7667. doi: [10.1162/089976600300014827](https://doi.org/10.1162/089976600300014827). eprint: <https://direct.mit.edu/neco/article-pdf/12/11/2519/814328/089976600300014827.pdf>. URL: <https://doi.org/10.1162/089976600300014827> (cit. on p. 5).
- Markram, H et al. (Jan. 1997). "Regulation of synaptic efficacy by coincidence of postsynaptic APs and EPSPs." en. In: *Science* 275.5297, pp. 213–215 (cit. on p. 10).
- Meunier, David et al. (2009). "Hierarchical modularity in human brain functional networks." In: *Frontiers in Neuroinformatics* 3. ISSN: 1662-5196. doi: [10.3389/neuro.11.037.2009](https://doi.org/10.3389/neuro.11.037.2009). URL: <https://www.frontiersin.org/articles/10.3389/neuro.11.037.2009> (cit. on pp. 1, 6).
- Nessler, Bernhard et al. (Apr. 2013). "Bayesian Computation Emerges in Generic Cortical Microcircuits through Spike-Timing-Dependent Plasticity." In: *PLOS Computational Biology* 9.4, pp. 1–30. doi: [10.1371/journal.pcbi.1003037](https://doi.org/10.1371/journal.pcbi.1003037). URL: <https://doi.org/10.1371/journal.pcbi.1003037> (cit. on pp. 1, 2, 15, 16, 18, 21, 27, 36, 67, 71).
- Palmer, Stephen (Jan. 1999). *Vision Science: From Photons to Phenomenology*. Vol. 1, p. 153 (cit. on p. 7).
- Parr, Thomas and Karl J. Friston (2018). "The Anatomy of Inference: Generative Models and Brain Structure." In: *Frontiers in Computational Neuro-*

## Bibliography

---

- science* 12. ISSN: 1662-5188. DOI: 10.3389/fncom.2018.00090. URL: <https://www.frontiersin.org/articles/10.3389/fncom.2018.00090> (cit. on pp. 1, 8).
- Pfister, Jean-Pascal and Wulfram Gerstner (2006). "Triplets of Spikes in a Model of Spike Timing-Dependent Plasticity." In: *Journal of Neuroscience* 26.38, pp. 9673–9682. ISSN: 0270-6474. DOI: 10.1523/JNEUROSCI.1425-06.2006. eprint: <https://www.jneurosci.org/content/26/38/9673.full.pdf>. URL: <https://www.jneurosci.org/content/26/38/9673> (cit. on pp. 11, 71).
- Pouget, Alexandre et al. (Sept. 2013). "Probabilistic brains: knowns and unknowns." In: *Nature Neuroscience* 16.9, pp. 1170–1178. ISSN: 1546-1726. DOI: 10.1038/nn.3495. URL: <https://doi.org/10.1038/nn.3495> (cit. on p. 8).
- Riesenhuber, Maximilian and Tomaso Poggio (2002). "Neural mechanisms of object recognition." In: *Current Opinion in Neurobiology* 12.2, pp. 162–168. ISSN: 0959-4388. DOI: [https://doi.org/10.1016/S0959-4388\(02\)00304-5](https://doi.org/10.1016/S0959-4388(02)00304-5). URL: <https://www.sciencedirect.com/science/article/pii/S0959438802003045> (cit. on p. 7).
- Rodney J Douglas, Kevan A C Martin (2004). "Neuronal circuits of the neocortex." In: *Annual review of neuroscience* 27, pp. 419–451. DOI: 10.1146/annurev.neuro.27.070203.144152 (cit. on pp. 2, 5).
- Taherkhani, Aboozar et al. (2020). "A review of learning in biologically plausible spiking neural networks." In: *Neural Networks* 122, pp. 253–272. ISSN: 0893-6080. DOI: <https://doi.org/10.1016/j.neunet.2019.09.036>. URL: <https://www.sciencedirect.com/science/article/pii/S0893608019303181> (cit. on p. 11).